Tutor/s

Dr. Federico Calle Vallejo
Department of Physical Chemistry

Grau en Enginyeria Química

Trabajo Final de Grado

CO Electro-oxidation using near-surface alloys of platinum and transition metals

Alvaro Brito Ravicini

June 2021

UNIVERSITAT DE BARCELONA

El conocimiento no es una vasija que se llena, sino un fuego que se enciende.

Plutarco

Quiero dedicar este trabajo a todas aquellas personas que han visto en mí, el potencial suficiente para darme una oportunidad. Voy a empezar por mis padres, ya que sin su apoyo y amor incondicional nada de esto hubiese sido posible. De hecho, quiero que consideren que este logro es tan mío como suyo. Agradezco a mi familia, que, si bien empezamos estando todas cerca, hoy en día, estamos esparcidos por el mundo, pero, aun así, tan unidos como al principio. Le quiero dar las gracias a mi tutor, Dr. Federico Calle Vallejo, por sugerirme este proyecto que empezó hace 2 años, y desde entonces me ha ayudado, guiado y motivado. Finalmente, agradezco a todos mis amigos tanto de Cataluña como de Venezuela, por la ayuda, el cariño, y el soporte que me han brindado por tantos años.

CONTENTS

SUMMARY

The purpose of this thesis is to analyze the trends of near-surface alloys (NSAs) of platinum and transition metals toward CO electro-oxidation to CO_2, in order to identify promising electrode materials to perform the reaction. To do so, Density Functional Theory (DFT) simulations were performed. This work is composed of two parts: the first part consists of modeling the reaction on the (111) facet of NSAs of platinum and transition metals, while the final part considers the (331) facet. The first part is subdivided into 5 sections: the first section introduces the surface that is going to be modeled as well as the target catalytic reaction. The second one shows the catalytic trends as a function of the number of valence electrons of the guest transition metal. The third one compares a simple adsorption model to a co-adsorption model. The fourth one examines whether linear scalability of the intermediates exists and provides volcano-type activity plots to determine promising candidates. Lastly, the fifth section deals with the effect of the transition metal coverage on the most active alloy. The composition of the second part is similar, except for the co-adsorption model and the analysis of coverage effects, which were not performed. The results reveal that the most promising alloys are the (111) facet of Pt-Mn NSAs and the (331) facet of Pt-Os NSAs.

Keywords: CO electro-oxidation, volcano-type activity plots, adsorption-energy scaling relations, electrocatalysis, DFT.

RESUMEN

El objetivo de este Trabajo Final de Grado (TFG) es analizar las tendencias en la actividad catalítica de las aleaciones cercanas a la superficie (Near-Surface Alloys/NSAs) de platino y metales de transición para la electro-oxidación de CO a CO_2, identificando de paso materiales prometedores para catalizar dicha reacción. El análisis se realizó a través de simulaciones de la teoría del funcional de la densidad (Density Functional Theory/DFT). Este documento consta de dos partes. La primera parte muestra la modelización de la reacción sobre la faceta (111) de aleaciones cercanas a la superficie de platino y metales de transición. En la segunda parte se emplean las mismas aleaciones, pero esta vez en la faceta (331). La primera parte se subdivide en 5 secciones: en la primera sección se introduce la superficie que se va a modelar, así como la reacción electrocatalítica. La segunda sección muestra las tendencias en función del número de electrones de valencia del metal de transición. La tercera sección compara un modelo de adsorción simple contra uno de co-adsorción. La cuarta sección examina si existen relaciones lineales entre las energías de adsorción de los intermediarios, y muestra gráficos de volcán para la actividad catalítica (volcano-type activity plots) que servirán para identificar aleaciones prometedoras. Finalmente, la quinta sección muestra el efecto de la cobertura del metal de transición sobre la aleación catalíticamente más activa. La estructura de la segunda parte del documento es similar a la de la primera, aunque no se llevó a cabo un estudio del efecto de la cobertura ni de co-adsorción en la faceta (331). El análisis muestra que las aleaciones más prometedoras para la electro-oxidación de CO son la NSA de Pt-Mn en la faceta (111) y la NSA de Pt-Os en la faceta (331).

Palabras clave: electro-oxidación de CO, gráficos de volcán para la actividad catalítica, relaciones de escala para energías de adsorción, electrocatálisis, DFT

1. INTRODUCTION

The direct electro-oxidation of carbon monoxide (CO) was first studied around a century ago [1], but it was not until the 1950-1960's that it was considered in the context of fuel cells. At the beginning, the studies on fuel cells were motivated by space and military applications.

The type of fuel cell where CO electro-oxidation is involved is known as a Direct Methanol Fuel Cell (DMFC), and early prototypes used alkaline electrolytes. Early on, research was focused on finding optimal materials for the electrodes to enhance reaction rates. Under alkaline conditions, it was shown that the best materials were a platinum-palladium alloy for the cathode, silver for the anode and potassium hydroxide for the electrolyte. The drawback of this precursor of the current DMFCs was the creation of carbonates due to the reaction of the alkaline electrolyte with carbon dioxide (CO_2). Carbonates poisoned the electrode and, even though cell regeneration was possible, its durability was severely compromised.

As a result of this poisoning, the interest shifted from CO electro-oxidation under alkaline conditions to acid pH. The materials commonly used were platinum for the electrodes and sulfuric acid as the electrolyte. However, in 1968 a Shell scientist identified a platinum-ruthenium alloy as an effective anode catalyst. To this date, this is the most common anode catalyst found in DMFCs. The last important change DMFCs suffered was the substitution of liquid electrolytes to solid acidic polymer membranes, which brought up a significant improvement in cell performance.

What began as alternative project to convert energy is now a necessity to confront current environmental challenges. The use of fossil fuels has allowed us to power our houses, cars, and industries, but at a tremendous environmental cost estimated around $5 trillion annually due to the increasing levels of pollutants in the atmosphere [2]. Fuel cells are environmentally-friendly, energy conversion devices that do not burn fossil fuels and promise to deliver high efficiencies and high energy densities at low maintenance costs.

DMFCs can be used for small, portable applications. Unfortunately, they currently suffer from low efficiencies caused by a number of reasons, namely, methanol crossover, water management, and high anodic overpotentials. The first two factors are intrinsic to the cell design, while the latter is related to materials selection. Lowering anodic overpotentials is the main scope of this work, and this formidable challenge is tackled from a computational materials design standpoint.

2. THEORETICAL BACKGROUND

2.1. BASIC DFT

To understand the main findings of this study it is not necessary to understand all the complexities of Density Functional Theory (DFT). However, a brief explanation of the main equations governing DFT is pertinent. The following section is based on previous works [3]. One of the key advances of the 20th century was the development of quantum mechanics, which allowed to describe matter with an extraordinary level of accuracy. This is brought up because to understand DFT, one must become familiar with some problems of quantum mechanics.

One of the properties that scientists are most interested in from a collection of atoms is their energy. To tackle this problem, the location of the atoms and their electrons must be known beforehand. One key observation is that the nuclei are considerably heavier than the electrons and, therefore, electrons respond more rapidly to changes in the environment compared to the nuclei. This allows physicists to solve the equation that describes electronic motion by fixing the position of the nuclei, which lets them calculate the minimum electronic energy configuration, known as the ground state of the electrons. This is called the Born-Oppenheimer approximation, and the function that describes the ground-state energy as a function of the position of the nuclei is known as the adiabatic potential energy surface of the atoms. Once this function is calculated, one can proceed to next step.

Now, what happens when atoms move? To address this problem, the non-relativistic and time independent Schrödinger Equation was introduced. The form of this equation depends on the physical system one wants to describe. The Schrödinger Equation is rather complex for systems containing several atoms, as it has to incorporate the interaction between multiple electrons and nuclei. This is shown in Eq. 2.1 for an electronic wave function in steady-state conditions:

$$\left[-\frac{h^2}{2m}\sum_{i=1}^{N}\nabla_i^2+\sum_{i=1}^{N}V(r_i)+\sum_{i=1}^{N}\sum_{j<i}U(r_i,r_j)\right]\psi=E\psi \qquad (2.1)$$

In Eq. 2.1 h is the Planck constant, m is the mass of an electron, ψ is the electronic wave function, which depends on each of the spatial coordinates of every single electron, and E indicates the ground-state energy. Inside the brackets from left to right, the terms describe the sum of the kinetic energies of the electrons, the electronic interaction between electrons and nuclei, and the electronic interactions between one electron and the rest.

If one examines Eq. 2.1 in detail, the conclusion is that solving this equation is an incredibly difficult task that requires the use of different approximations. One of them is the Hartree product, which defines the wave function as a product of individual electron wave functions. The complexity of the resolution arises from the size of the wave function, and the fact that it is a many-body problem. For instance, solving Eq. 2.1 for a simple molecule such as H_2O implies that the wave function is a 30-dimensional function, since water has 10 electrons, and each of them has three spatial coordinates (x,y,z). Besides, the third term inside the brackets in Eq. 2.1, which describes electronic interactions, cannot be computed for an individual electron wave unless the individual electron wave function for the rest of electrons is known.

Although there is much interest on calculating the wave function, most of its information cannot be directly observed. Nevertheless, one thing that can be measured and contains a lot of information of an atomic system, is the electronic density. This density is a three-dimensional function that describes the probability that N electrons are at a particular set of coordinates, and is formulated as Eq. 2.2:

$$n(r)=2\sum_i \psi_i^*(r)\psi_i(r) \qquad (2.2)$$

Where $\psi_i^*(r)\psi_i(r)$ denotes the probability that an electron is at a given coordinate (r), and it is the product of the individual electron wave function and its conjugate. The factor 2 is due to the spin of the electrons and the Pauli exclusion principle, which establishes that each individual electron wave function can be occupied by two electrons only if they have different spin.

The core of DFT is composed of two theorems by Kohn and Hohenberg, and the set of equations derived by Kohn and Sham. The first theorem of Kohn and Hohenberg states that there exists a one-to-one relation between the ground-state energy of the wave function and the

ground-state electronic density. Importantly, this theorem describes the ground-state energy as a function of the electronic density, which is a three-dimensional function. Even though the first theorem states the existence of a relation (functional), it does not establish it. The second theorem outlines an important feature of the density functional: "the electron density that minimizes the energy of the overall functional will be the true electron density corresponding to the full solution of the Schrödinger equation"[3]. Hence, if the functional is known, finding the ground state is only a matter of optimization.

To write the Hohenberg-Kohn theorem, it is useful to remember that the electron density can be written in terms of single-electron wave functions (Eq. 2.2), which leads to Eq. 2.3:

$$E[\psi_i]=E_{known}[\psi_i]+E_{XC}[\psi_i] \tag{2.3}$$

The energy is divided into two terms: one of them is known and can be written analytically, while the other contains all the unknown information and is called the exchange-correlation functional. The known term can be expressed as a series of contributions (Eq. 2.4):

$$E_{known}[\psi_i]= -\frac{h^2}{m}\int \psi_i^* \nabla^2 \psi_i d^3r + \int V(r)n(r)d^3r + \frac{e^2}{2}\int\int \frac{n(r)n(r')}{|r\ r'|} d^3r\, d^3r' + E_{ion} \tag{2.4}$$

The first term refers to the kinetic energy of the electrons, the second term indicates the Coulomb interaction between electrons and nuclei, the third one incorporates the Coulomb interaction between the electrons and the fourth one specifies the Coulomb interaction between nuclei.

The logic behind the Kohn-Sham equations is that the minimum electronic density can be calculated through a set of equations that involve only a single electron. These equations look like Eq. 2.5:

$$\left[-\frac{h^2}{m}\nabla^2+V(r)+V_H(r)+V_{XC}(r)\right]\psi_i(r)=\varepsilon_i\psi_i(r) \tag{2.5}$$

It is worth noting that Eq. 2.1 and Eq. 2.5 are similar. The left-hand side of Eq. 2.5 contains three terms inside a bracket operating over the wave function of a single electron, which only depends on three spatial coordinates. Inside the bracket, there are three potentials V, V_H, and V_{XC}. The first one appeared both in Eq. 2.1 and Eq. 2.4 and denotes the interaction between an electron and a collection of nuclei. The second one is the Hartree potential, which describes the Coulomb repulsion that a given electron experiences from the total energy density defined by

considering all the electrons. This includes a self-interaction term because a given electron is part of the total electronic density. The mathematical expression for the Hartree potential is (Eq. 2.6):

$$V_H(r)=e^2 \int \frac{n(r')}{|r\ r'|}\, d^3r' \tag{2.6}$$

The last potential in Eq. 2.5 is V_{XC}, which is the functional derivative of the Exchange Correlation energy defined as (Eq. 2.7):

$$V_{XC}(r) = \frac{\delta E_{XC}(r)}{\delta n(r)} \tag{2.7}$$

The issue with Eq. 2.5 is that in order to solve the problem, the Hartree potential must be defined, but to do so, the electron density needs to be known, which is a function of the single electron wave functions that are the solutions of Eq. 2.5. To mathematically solve this problem, an iterative algorithm is used that follows these general guidelines:

- Suppose an initial electron density n(r).
- Find the individual electron wave functions, $\psi_i(r)$, from the assumed electron density and the Kohn-Sham equations (Eq. 2.5).
- From the individual wave function, $\psi_i(r)$, calculate the electron density through Eq. 2.2.
- Compare the calculated electron density with the intial one. If they coincide, the ground state electron density was found, and it can be used to calculate the total energy. If not, the electron density must be updated, and the process is repeated starting at step 2.

To sum up the DFT fundamentals, a concept introduced before must be defined, which is the exchange-correlation functional. Even though its existence is known, physicists have no clue of how it is defined mathematically speaking. There is just one case, where they have derived this functional, which is the uniform electron gas. In that case, the electron density is constant everywhere in space. Knowing this, the exchange correlation potential can be approximated to that of a uniform gas at a particular observed point (Eq. 2.8), allowing us to solve the Kohn-Sham equations (Eq. 2.5):

$$V_{XC} = V_{XC}^{electron\ gas}[n(r)] \tag{2.8}$$

The use of the local density to compute the exchange correlation functional is called the local density approximation (LDA). Other well-known exchange correlation functionals are those calculated from not only the local electron density, but also the local gradient in the electron density. Such functionals are known as generalized gradient approximation (GGA) functionals. In this work we used the Perdew-Burke-Ernzerhof functional [19], which is the most widely used GGA functional.

2.2. VASP

During the elaboration of this thesis, a simulation package was used to carry out the DFT calculations. One of the simulation packages available at the University of Barcelona is the Vienna Ab Initio Simulation Package (VASP) [18].

Before accessing the simulator, it is crucial to learn the fundamentals of Bash, which is the programming language used by Linux. Bash is a command interpreter, which means that it interacts with the computer operating system. The simulations are not performed in a personal computer, instead they are executed in a supercomputer. To access it, Bash programming is required. To use VASP, one must be able to perform the following tasks with Bash:

- Directory navigation.
- Basic file operations.
- File viewing and editing.
- Shell scripting (not necessary, but highly recommended).

When using VASP, one must find out which files are necessary for the simulation (input files), and which ones contain the results of the calculations (output files). To compute a simulation, one needs five files: POSCAR, INCAR, POTCAR, KPOINTS and a submission script. In this document, a rigorous explanation for each file will not be given, instead a brief overview of the purpose of each file in the simulation will be mentioned. For more information, regarding a particular file, one can access the VASP Manual [4].

The POSCAR file defines the atomic coordinates and degrees of freedom of all the atoms in the simulation, the lattice vectors, the atomic species present and their number. The order of the species must be consistent with the order in the POTCAR, otherwise, there will be errors in the calculations. The POTCAR file contains information on how core and valence electrons of all

species will be represented. In this study the projector augmented-wave method was used [17]. The KPOINTS file states the number of k-points used to perform the calculations in the reciprocal space. To generate those, we used the Monkhorst-Pack scheme [20].The parameters used in the simulations are the INCAR file, which defines the details of the calculations such as: type of calculation (single-point calculation, full relaxation, frequency analysis, etc.), step size, optimization algorithm, convergence criteria for ionic and electronic loops, and output file generation, among others. Finally, the submission script declares the version of VASP employed, the maximum calculation time, the number of cores to be used, a name for the calculation, and sends the calculation to the supercomputer queue.

There are more output files than input files; however, only the two most important ones for our purposes are the OUTCAR and the CONTCAR files. The OUTCAR file is the main output file and contains information about the input parameters, energy and Fermi level at every electronic step, Kohn-Sham eigenvalues, stress tensors, forces in atoms, local charges, and several other things. The CONTCAR file contains the final geometry of the calculation.

2.3. BASIC THERMODYNAMICS

The Gibbs Free energy of a reaction is defined as the energy difference between reactants and products. For a given chemical reaction, namely Eq. 2.9, reactants R_i (i: can range from 0 to the total number of reactants (N)) combine to give products P_j (j: can range from 0 to the total number of products (M)), each multiplied by its correspondent stochiometric coefficient (α_i for reactants, and γ_j for products). The Gibbs free energy of reaction is shown in Eq. 2.10. Furthermore, if the reaction energy is calculated at standard conditions (298.15 K and 1 atm), then it is deemed the standard Gibbs energy of reaction [5].

$$\alpha_1 \cdot R_1 + \alpha_2 \cdot R_2 + \ldots + \alpha_N \cdot R_N \rightarrow \gamma_1 \cdot P_1 + \gamma_2 \cdot P_2 + \ldots + \gamma_M \cdot P_M \tag{2.9}$$

$$\Delta_r G = \sum_{j=0}^{M} \gamma_j \cdot G_{P_j} - \sum_{i=0}^{N} \gamma_i \cdot G_{R_i} \tag{2.10}$$

An important parameter of an electrochemical cell is its cell potential (E), which is defined as the potential difference between the two electrodes. This value gives an idea of the amount of electrical work a cell can achieve, which through Nernst equation (Eq. 2.11) can be related to the composition of the species at the cell and the standard Gibbs energy of reaction (Eq. 2.12)

[6]. To understand Eq. 2.12 two terms must be defined. The standard cell potential (ΔE^0_{cell}) is the cell potential when all the reactants and products are in their reference state [6]. The reaction quotient (Q) is defined as the ratio of the activities of products over those of the reactants to the power of their corresponding stochiometric coefficient [25].

$$\Delta E_{cell} = \Delta E^0_{cell} - \frac{R \cdot T}{v \cdot F} \cdot \ln(Q) \tag{2.11}$$

$$\Delta_r G^0 = -v \cdot F \cdot \Delta E^0_{cell} \tag{2.12}$$

In this equation, F is the Faraday constant and v the number of electrons transferred. Galvanic electrochemical devices have positive cell potentials. From Eq. 2.11 and Eq. 2.12 it is clear that to have a functional galvanic cell, it is mandatory that the cell reaction is spontaneous ($\Delta_r G^0 < 0$), because in that case $\Delta E^0_{cell} > 0$.

One of the results obtained from a DFT simulation is the total energy of an intermediate; however, this is not a Gibbs free energy. It is regarded as the DFT energy and is related to the Gibbs Free energy through Eq. 2.13 [7].

$$G = E_{DFT} + ZPE - TS + E_{solv} \tag{2.13}$$

From Eq. 2.13, it is possible to deduce that DFT energies and Gibbs energies of adsorption are connected through a series of corrections made to the adsorbates and the free molecules involved in the reaction. The ZPE term is the zero-point energy correction and is obtained by performing vibrational analysis. The next term is the product of the temperature and the entropy, it only considers the vibrational entropy of the adsorbates and the total entropy of the molecules (obtained from thermodynamic tables [9]). Finally, E_{solv} is the solvation effect the adsorbates experience from the solvent molecules, and the values utilized in this paper were extracted from other works [9, 10].

2.4. TAFEL KINETICS

Julius Tafel studied the hydrogen evolution reaction (HER) on metals. From the experimental data, he observed that far from the equilibrium potential, a logarithmic law between the overpotential and the current is obeyed (see Eq. 2.14). The overpotential is the potential difference from the equilibrium required to overcome the activation energy of the reaction to produce a specific current [26]. Bulter, Volmer and co-workers derived an

electrochemical rate equation that describes the kinetic behavior of electrodes as a function of the potential, where j_0 is the exchange current density, R is the gas constant, η is the overpotential, and α is the charge transfer coefficient (see Eq. 2.15) [11].

$$\eta = a + b \log j \tag{2.14}$$

$$j = j_F - j_R = j_0 \exp\left(\frac{\alpha \eta F}{RT}\right) - j_0 \exp\left(\frac{-(1-\alpha)\eta F}{RT}\right) \tag{2.15}$$

The two terms in the Bulter-Volmer equation correspond to the forward and backward reactions. For large values of overpotential the electrode reaction becomes irreversible, and Butler-Volmer equations is simplified to the Tafel equation.

2.5. BASIC PRINCIPLES OF FUEL CELLS

In broad terms, a fuel cell consists of two electrodes separated by an electrolyte (see Fig. 2.1). A fuel is fed to the anode, while an oxidant is supplied to the cathode. Through electrochemical reactions the cell can transform the chemical energy contained in the fuel directly into electric energy. The fact that this conversion is done directly means that electrochemical devices are not subjected to the Carnot efficiency. The theoretical maximum efficiency a fuel cell can achieve at standard conditions is given by Eq. 2.14:

$$\varepsilon = \frac{-2 \cdot F \cdot \Delta E^0}{\Delta H} \tag{2.16}$$

where ΔH is the enthalpy change of the reaction. The maximum efficiency cannot be achieved due to voltage loses caused by electrode polarization, internal and external cell resistances, and mass transport limitations. Electrode polarization occurs when current flows and causes overpotential. Overpotential is the deviation of the electrode potential from the standard potential, and this affects the amount of electric work the cell can perform. Ohmic voltage losses are due to two factors: the resistance of the electrolytes connecting the electrodes and the electronic resistance associated with the electrode connections [2].

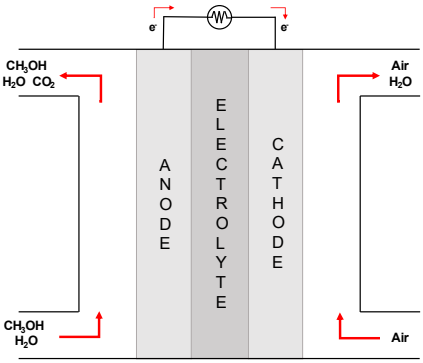

Figure 2.1. Schematic diagram of a direct methanol fuel cell. Adapted from [2].

2.6. ANODIC OXIDATION OF METHANOL

In DMFCs, methanol oxidation can be summarized in three main processes [12]. The first one is the electrosorption and dehydrogenation of methanol onto the electrode, the second consists of the subsequent addition of OH, and the third is the recombination of both producing CO2. Only a few electrodes are capable of adsorbing methanol, and they are usually made of pure platinum and its alloys. On platinum, the underlying mechanism of methanol oxidation consists of a series of dehydrogenation steps (Eq. 2.17-20).

$$Pt + CH_3OH \longrightarrow Pt\text{-}CH_2OH + H^+ + e^- \quad (2.17)$$

$$Pt\text{-}CH_2OH \longrightarrow Pt_2\text{-}CHOH + H^+ + e^- \quad (2.18)$$

$$Pt_2\text{-}CHOH \longrightarrow Pt_3\text{-}COH + H^+ + e^- \quad (2.19)$$

$$Pt_3\text{-}COH \longrightarrow Pt\text{-}CO + 2Pt + H^+ + e^- \quad (2.20)$$

The first steps of the reaction (Eq. 2.17-20) are rapid compared to last one. Therefore, the major species on the surface will be Pt-CO (CO adsorbed on Pt). The second part of the methanol oxidation reaction is the formation of Pt-OH, as shown in Eq. 2.21:

$$Pt + H_2O \longrightarrow Pt\text{-}OH + H^+ + e^- \quad (2.21)$$

The last step is the reaction between neighboring Pt-OH and Pt-CO to produce CO_2 following Eq. 2.22.

$$Pt\text{-}OH + Pt\text{-}CO \rightarrow 2Pt + CO_2 + H^+ + e^- \quad (2.22)$$

The catalytic activity of platinum toward methanol electro-oxidation is not optimal, which causes low efficiencies. Nonetheless, there are ways to promote its activity, and one of them is metal alloying, as explained in the next pages.

3. OBJECTIVES

The main aims of this work are:

- To determine promising material candidates for CO electro-oxidation.
- To evaluate the effect coordination on the catalytic activities.

To do so, Density Functional Theory (DFT) calculations are used to obtain activity trends for the different materials and surface facets. The specific objectives are to:

1. Determine the total energy of the clean surfaces.
2. Calculate the adsorption energies of the reaction intermediates.
3. Analyze activity trends as a function of the number of valence electrons.
4. Determine possible scaling relationships between reaction intermediates.
5. Construct contour plots based on adsorption energies to identify promising materials.

4. CATALYTIC ACTIVITY OF NEAR SURFACE ALLOYS OF PLATINUM (111) AND TRANSITION METALS

4.1. INTRODUCTION

The use of pure metals as catalysts may be optimal for certain scenarios; however, for most it has proven better to use alloys because of their reactivity and flexibility [27]. The presence of an alloying metal on a substrate produces interactions that increase or decrease catalytic reactivity due to primarily three effects: ensemble, ligand, and geometric effects [27]. Alloys can be prepared in different ways, in this work a near-surface configuration was chosen in which the alloying metal is located only at the subsurface. For DFT modelling, this means that the catalysts are modeled as a 4-layer metal slab, in which the second layer is occupied by a guest atom and the rest is platinum (Fig. 4.1).

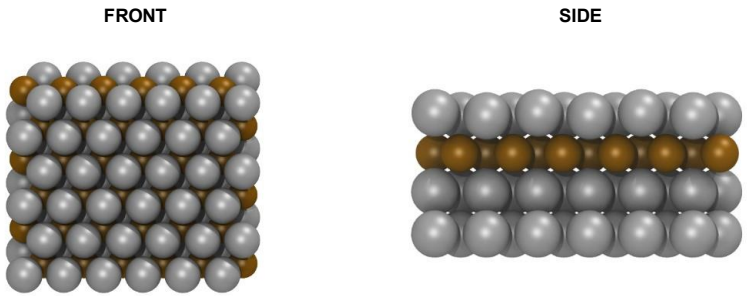

Figure 4.1. Structure of a (111) Pt-Cu NSA. Each subplot represents a different view of the same cell, as indicated by the labels. The color code used is ochre for Cu and silver for Pt.

To model CO electro-oxidation, a reaction mechanism is necessary. Based on previous scientific articles on the subject [9], the following mechanism was chosen (Eq. 4.1-3):

$$CO_{(g)} + * \rightarrow *CO \quad (4.1)$$

$$H_2O_{(l)} + * + *CO \rightarrow *CO + *OH + H^+ + e^- \quad (4.2)$$

$$*OH + *CO \rightarrow CO_{2\,(g)} + 2* + H^+ + e^- \quad (4.3)$$

The asterisk (*) symbol represents a free site on the catalyst, while the *X convention represents a compound X bonded to such free site. The sum of all steps (4.1-4.3) equals the following global reaction (Eq. 4.4):

$$CO_{(g)} + H_2O_{(l)} \rightarrow CO_{2\,(g)} + 2\cdot(H^+ + e^-) \quad (4.4)$$

The intermediates (*CO, *OH) are adsorbed on the surface, and using DFT it is possible to calculate their total energies. Simulations must be performed to determine the site where adsorption will most likely occur. In a 2×2 (111) surface, eight possible sites for adsorbate binding exist (2 top sites, 2 bridge sites, 2 fcc hollow sites, 2 hcp hollow sites). According to experiments [9], *CO and *OH are atop adsorbates on Pt. In Fig. 4.2-3, different views of the surface structure including *CO and *OH in their corresponding adsorption site are shown.

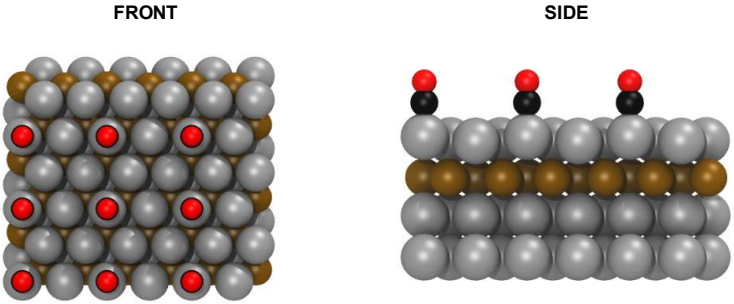

Figure 4.2. Geometric configuration of a (111) Pt-Cu NSA with CO adsorbed on atop. Each subplot represents a different view of the same cell. The color code used is ochre for Cu, silver for Pt, black for C and red for O.

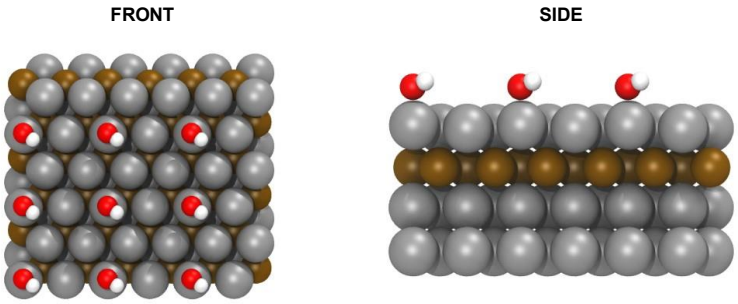

Figure 4.3. Geometric configuration of a (111) Pt-Cu NSA with OH adsorbed atop. Each subplot represents a different view of the same cell. The color code used is ochre for Cu, silver for Pt, white for H and red for O.

With a reaction pathway and a cell structure defined, the only step left is to carry out the calculations using VASP. The catalytic trends obtained from DFT are analyzed by means of two descriptors, namely, the number of valence electrons and the adsorption-energy scaling relations between the intermediates.

4.2. ANALYSIS BASED ON NUMBER OF VALENCE ELECTRONS

The number of valence electrons is a simple yet powerful tool that provides valuable information about the stability of molecular systems [13]. Thus, it is interesting to see whether this descriptor could capture the catalytic trends of CO electro-oxidation among (111)-NSAs.

To study the catalytic activities, it is necessary to calculate the Gibbs Free Energy of the reaction steps (Eq. 4.1-3). With these energies and the standard cell potential, the overpotential can be easily calculated (as shown in Eq. 4.5). In Fig.4.4, it is shown how the Gibbs Free Energy and the overpotential vary with the number of electrons for a given series of transition metals (3d).

The Gibbs free energy of step 1 (Eq. 4.1) corresponds to CO adsorption (ΔG_{CO}), and that of step 2 (Eq. 4.2) is *OH adsorption (ΔG_{OH}). They are calculated as indicated in Eq. 4.5-7:

$$\Delta G_1 = G_{*CO} - G_{CO} - G_* \quad (4.5)$$

$$\Delta G_2 = G_{*OH} + G_{H^+ + e^-} - G_{H_2O} - G_* \quad (4.6)$$

$$\Delta G_3 = G_{*CO_2} + G_{H^+ + e^-} - G_{*OH} - G_{*CO} \quad (4.7)$$

To find the Gibbs free energy of steps 2 and 3, the energy of the protons and electrons needs to be evaluated. To do so, the computational hydrogen electrode (CHE) is employed [7].

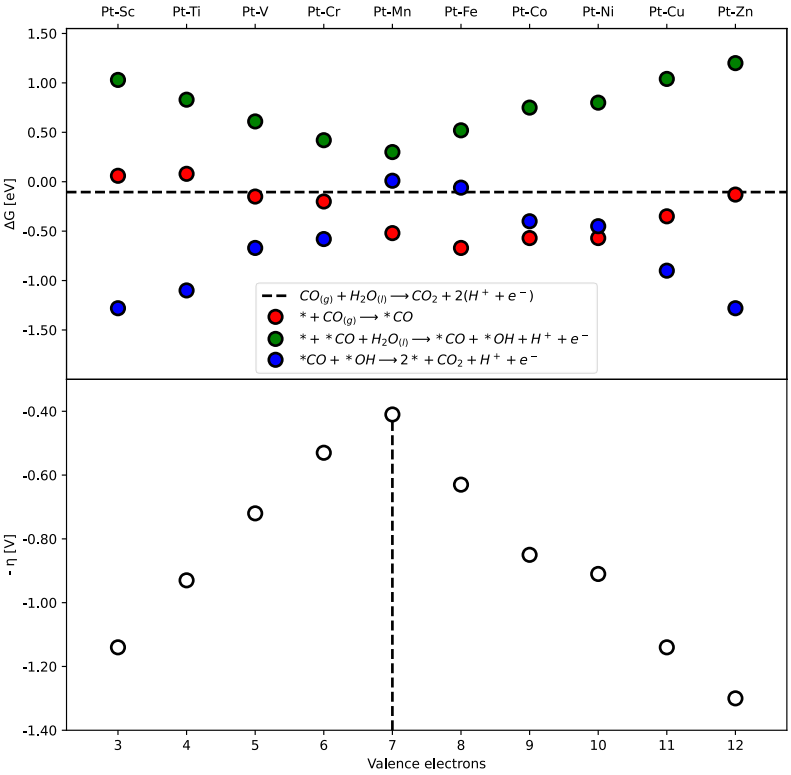

Figure 4.4. (a) Gibbs free energy for each step of the electro-oxidation of CO as a function of the number of valence electrons for (111)-NSAs composed of Pt and 3d metals. (b) Valence electron-activity plot for CO electro-oxidation. The optimal alloy has 7 valence electrons. The overpotential is calculated as $\eta = \frac{\max(\Delta G_2, \Delta G_3)}{e^-} - \Delta E^0$.

Analogous to Fig. 4.4, it is possible to make the same analysis for the 4d and 5d series of transition metals, see the Appendix 1 (A.1, A.2). Note that the trends and discussion provided here also applies to those.

The number of valence electrons is calculated for the guest atom in the alloy and is done considering the number of electrons in the s- and d-bands. For example, in a Pt-Mn NSA, the manganese atoms have the following electronic configuration: [Ar] $3s^2$ $4d^5$. The addition of the 2 electrons from the s orbital and the 5 electrons from the d orbital gives a total of 7 valence electrons. The s electrons are included in the count because some elements such as Pt have s^1 configurations instead of s^2.

From Fig.4a, it is interesting to note that regardless of the number of valence electrons, the Gibbs free energy of *OH (datapoints in green) is higher than that of *CO (datapoints in red). This means that *CO adsorption is more favorable than *OH adsorption, which could explain why Pt-based catalysts habitually experience *CO poisoning.

Through the Gibbs free energy for each reaction step at a given number of valence electrons and the equilibrium potential (-0.105 V), it is possible to calculate the overpotential from Eq. 4.8 (the first step is not included because it is not electrochemical):

$$\eta = \frac{\max(\Delta G_2, \Delta G_3)}{e^-} - \Delta E^0 \tag{4.8}$$

The overpotential allows to compare the catalytic activity of different alloys because it quantifies the excess energy required relative to the thermodynamic limit. In general, a higher overpotential translates into a lower cell energy; therefore, the goal is to identify materials with the lowest possible overpotential.

There exists a relationship between the form of the valence electron activity plot and the Gibbs free energy for each step (Fig. 4.4). Through Eq. 4.8 it is evident that the overpotential trends are given by the Gibbs energy of *OH. In the volcano plot in Fig. 4.4b, it is indicated through a dashed line the best (111)-NSA for a given energy level. For 3d metals it is the (111) Pt-Mn NSA. All the metals to the right or left of Mn in the volcano plot bind *OH too weakly, which slows down the reaction. In this case, the most active metals are the ones that bind *OH strongly.

A key concept in inorganic chemistry is that when a molecular system resembles the electronic configuration of a noble gas the stability is optimized. An easy way to apply this concept is through the 8 and 18 electron rules. This model has proven successful for identifying

the most stable alloys for other adsorbates [14]. In Fig. 4.5-7, the Gibbs free energies of *OH and *CO adsorption are plotted as a function of the number of valence electrons.

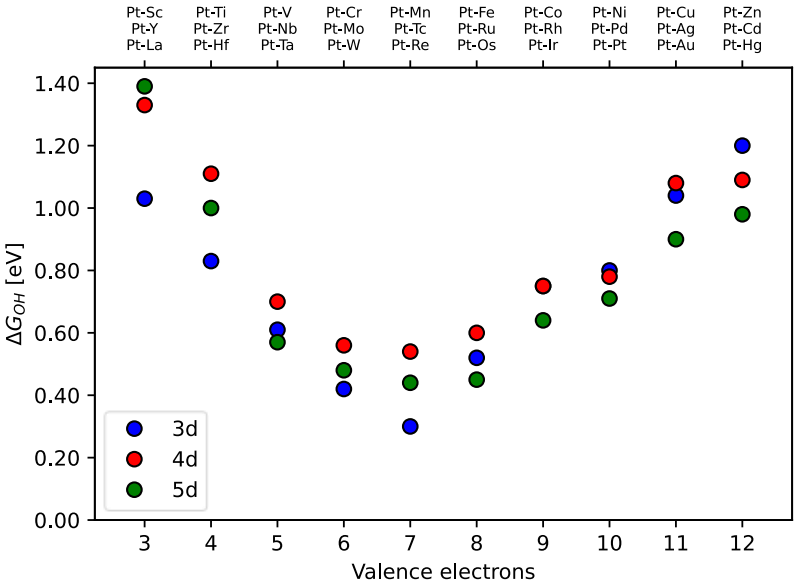

Figure 4.5. Comparison of *OH adsorption energy for alloys of different d series. The minimal *OH adsorption energy corresponds to 7 valence electrons for 3d, 4d, 5d transition metals.

The comparison of *OH adsorption energies shows that the shape of the energetic curve as a function of the number of valence electrons depicts a shallow V-shaped trend regardless of the d series of the guest atom. The criteria used to determine the most stable surface is to apply the 8-electron rule to the adsorbate, and the 18-electron rule to the surface components [14]. From a simple Lewis Diagram (Fig. 4.6), one can determine the electronic structure that resembles a noble gas for *OH adsorption, and it is the one where the guest metal has 7 valence electrons. Consequently, the most stable Pt NSAs for OH adsorption are Mn, Tc and Re. As Fig. 4.5 illustrates, this stability criteria describes well all the datapoints.

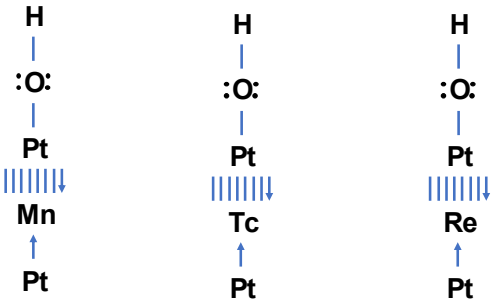

Figure 4.6. Lewis Diagrams for the OH-Pt-X system. The guest atoms (X) stabilize the electronic configuration, providing the system with a lower Gibbs free energy. The symbols indicate shared pairs of electrons (lines), lone pairs (dots) and dative bonds (arrows). Adapted from [14].

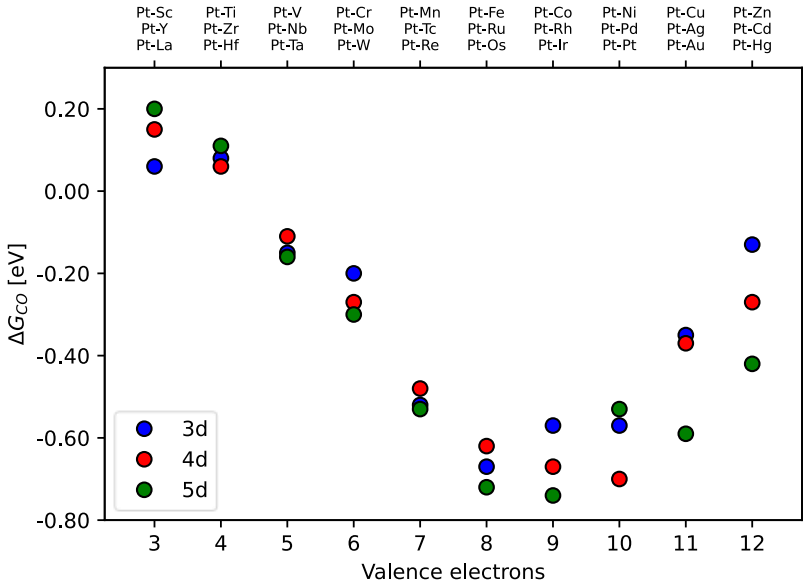

Figure 4.7. Comparison of *CO adsorption energy for alloys of different transition metal series. The minimum CO adsorption energy is around 8 valence electrons

*CO adsorption energies show a similar shape regardless of the d series considered. Applying the 8- and 18-electron rules describes well the 3d metals, but less so the 4d and 5d metals (see Fig. 4.7). For those metals, it is observed that the minima fall in the vicinity of 8

electrons, and the differences between such minima and the theoretical one (the one at 8 electrons) are not large. The Lewis Diagrams for this molecular system shows that the most stable surface is one where the guest atom has 8 valence electrons (see Fig. 4.8).

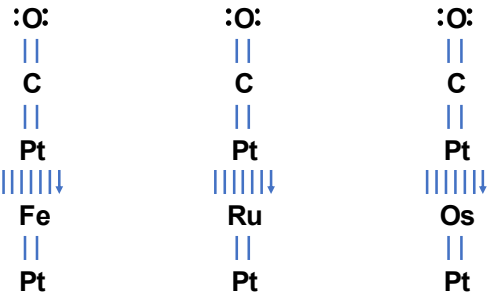

Figure 4.8. Lewis Diagrams for the CO-Pt-X system. The guest atoms (X) stabilize the electronic configuration providing the system with a lower Gibbs free energy. The symbols indicate shared pairs of electrons (lines), lone pairs (dots) and dative bonds (arrows). Adapted from [14].

A clarification must be made for (111) Pt-La NSAs. From basic inorganic chemistry [13], it is known that there is a general decrease in size from left to right and from bottom to top in the periodic table. An important factor that determines the feasibility of an alloy of certain composition is the size comparison between guest and host atoms. Ideally, for 50:50 alloys, the atoms should have similar sizes, since that leads to structurally stable alloys. Lanthanum is the largest transition metal, and when it was added to platinum the cells experienced problems converging and appreciable distortions were observed. While for the rest of alloys a criterion of 0.05 eV/Å was used for the forces, for Pt-La a criterion of 0.1 eV/ Å was employed.

4.3. COMPARISON BETWEEN SEPARATE ADSORPTION AND COADSORPTION

Up to this point, the adsorption steps were computed separately. This means that the effects of adsorbate-adsorbate interactions have not been considered. To do so, *CO and *OH must be simultaneously adsorbed on the surface. The first step of the reaction (*CO adsorption) does not require coadsorption, but the second and the third one do since *OH adsorbs once *CO has been adsorbed.

Coadsorption requires more computational resources; nonetheless, it should fit experimental data better, since these adsorbates coexist on the surface during experiments. This implies that when two adsorbates are in a surface the total energy of adsorption is not simply the energy of the metal and the adsorbate, but the interaction energy between the species also plays a role. In Fig. 4.9, it is shown the surface structure of a (111) platinum-transition metal with *CO and *OH coadsorption.

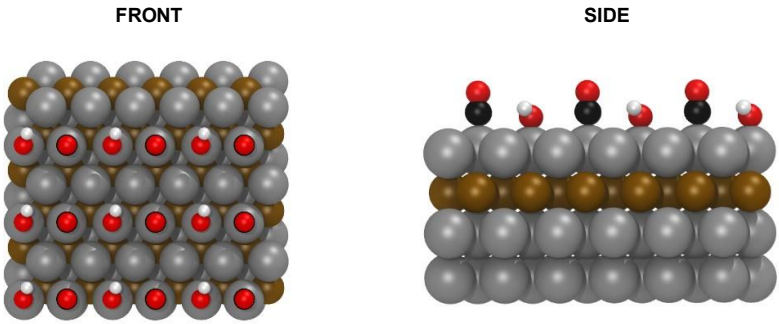

Figure 4.9. Geometric configuration of a (111) Pt-Cu NSA with CO and OH coadsorption. Each subplot represents a different view of the same cell. The color code used is ochre for Cu, silver for Pt, white for H, black for C and red for O.

When modeling coadsorption there are two possibilities: the H atom in the OH adsorbate is pointing towards the *CO, or it is not. To determine which representation is correct, one must compare the energetics of both systems. The one with the lowest Gibbs free energy for a given valence electron is the correct configuration. The non-facing adsorbates showed lower Gibbs Free energy for every single valence electron. This seems to follow general chemistry guidelines, which state that the optimal spatial configuration is the one that minimizes repulsions between species.

The catalytic activities including coadsorption are calculated analogously to simple adsorption. Fig. 4.10 shows how the Gibbs energy varies as a function of the number of valence electrons, while in Fig. 4.11 the relation between the overpotential and the number of valence electrons is plotted. Since the observations are similar for 4d and 5d metals, the figures will not be included in this section but at the Appendix 1 (A.3 and A.4).

The results show that the behavior of coadsorbed species is comparable to that of separate adsorbates since the shape of the trends is approximately the same. The only difference is the actual values of the Gibbs free energies, which stems from adsorbate-adsorbate interactions.

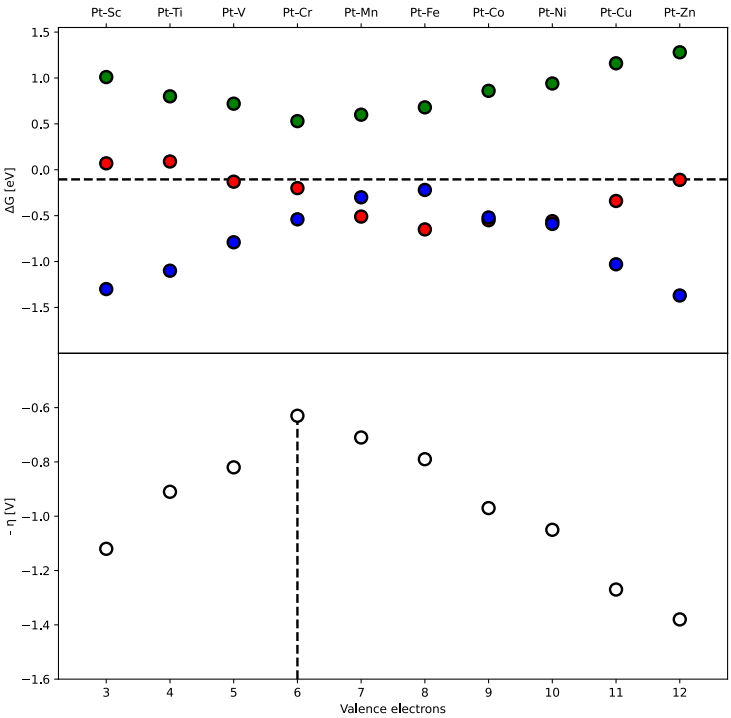

Figure 4.10. (a) Gibbs free energy for each step of the electro-oxidation of CO as a function of the valence number for (111)-NSAs of Pt and 3d metals considering adsorbate interactions. (b) Valence electron-activity plot for CO electro-oxidation considering adsorbate interactions. The optimal alloy has 6 valence electrons. The overpotential is calculated as $\eta = \frac{\max(\Delta G_2, \Delta G_3)}{e^-} - \Delta E^0$.

Comparing Fig. 4.4 and 4.10, the only points that differ appreciably are those of Pt-Mn and Pt-Cr alloys. This gives rise to a volcano plot, which follows the general shape of that of Fig. 4.4.b except for these alloys; therefore, showing a different optimal material. However, the differences are not large.

The importance of these results is that there exists an energetic shift, which corresponds to the adsorbate-adsorbate interactions. If this shift is calculated, it could be possible to obtain decent results from simpler, separate-adsorption models that would only require the addition of a correction.

To find the energetic shift, the Gibbs free energy of the second step of the reaction (Eq. 4.2) is plotted considering adsorption and coadsorption as a function of the number of valence electrons (see Fig. 4.11).

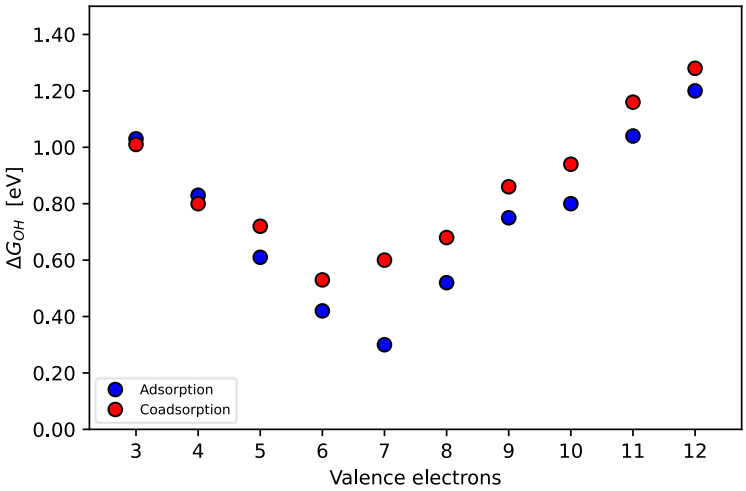

Figure 4.11. Comparison between *OH adsorption and *OH coadsorption with *CO for NSAs of Pt and 3d transition metals. There is on average an energetic shift of 0.11 eV.

The graphs for the 4d and 5d transition metals are in Appendix 1 (A.5 and A.6). To quantify the energetic shift, the difference between the coadsorption energy and the adsorption energy for every transition metal was considered. The average of these differences is 0.10 eV with a standard deviation of ± 0.06 eV.

4.4. ANALYSIS BASED ON SCALING RELATIONS

Scaling relations are a key finding within the field of surface science and heterogenous catalysis [21]. The underlying idea behind them is that if the energetic curves of two adsorption energies exhibit a similar behavior as a function of the same descriptor, they must be linearly related [7,14] (see Eq. 4.9).

$$\Delta G_{CO} = \gamma \cdot \Delta G_{OH} + \varepsilon \tag{4.9}$$

Not all adsorption energies scale linearly with each other. A way of knowing this is through the analysis of the critical points of the energetic curves (minimum, maxima, or saddle points). A requirement for a smooth overlap is that both functions must share the same critical points [14].

Based on the above, it can be anticipated that the Gibbs free energies of *CO and *OH will not scale since they do not share a common minimum (for *OH, it is 7 valence electrons, while for *CO, it is 8 valence electrons. This is shown in Fig.4.5 and 4.7). This is confirmed in Fig. 4.12, where the adsorption energy of *CO is plotted as a function of the *OH adsorption energy.

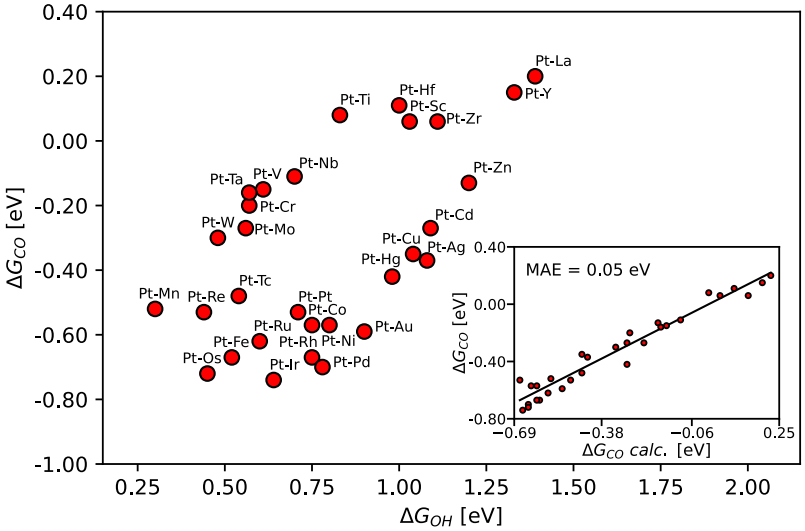

Figure 4.12. *CO adsorption energies vs *OH adsorption energies for (111)-NSAs of Pt and transition metals. There is no linear scaling between the adsorption energies. Inset: DFT-calculated adsorption energy of *CO (y-axis) plotted against predicted *CO adsorption energy (x-axis). The CO adsorption energies are fitted to a 3rd degree order polynomial. The MAE is only 0.05 eV.

There is, however, a way to deal with non-scalability. Following closely the procedure of [14], it is possible to fit the adsorption energies to a third order polynomial with respect to a given electronic structure parameter (here chosen to be the number of valence electrons). From this fit, one can calculate the energetics of the other intermediate using the following equation:

$$\Delta G_1 = \gamma \cdot \Delta G_2 + \sum_{j=0}^{3} [\alpha_j \cdot \omega_{T1}^j - \gamma \cdot \beta_j \omega_{T2}^j] \quad (4.10)$$

Eq. 4.10 originates from the substitution of Gibbs free energy terms in Eq. 4.9 by the third order polynomial. The parameters α_j and β_j refer to coefficients of the third order polynomial, γ is the slope of the scaling relation, and ω_T is the descriptor (number of valence electrons). If the polynomial fits the data well, then through Eq. 4.10 one can calculate the Gibbs free energy of one intermediate as a function of the other and a series of parameters. The value of γ can be evaluated as the relation between the number of bonds that species 1 lacks to reach the octet and the number of bonds that species 2 lacks to reach the octet. In this case, the O atom in *OH lacks one bond to reach the octet, while the C atom in CO needs two, so γ = ½.

From the inset in Fig. 4.12, it is seen that for a γ value of ½ and for the respective regression parameters, the predictions of Eq. 4.10 described the data obtained from DFT reasonably well. Indeed, the Mean Absolute Error (MAE) is of 0.05 eV for the fit.

Since *CO and *OH do not scale linearly with each other on (111) Pt-based NSAs, a 3D volcano plot is to be constructed that relates the Gibbs free energy of these two intermediates with the overpotential. The construction of this figure is analogous to that of [15].The procedure is relatively simple and only requires knowledge of the Gibbs energy of the reaction.

The reaction mechanism is composed of a series of steps (Eq. 4.1-3); however, from general thermodynamics, it is known that the presence of a catalyst should not affect the overall reaction thermodynamics. Therefore, the summation of the Gibbs free energy of step 1, 2, and 3 must always be equal to the Gibbs energy of the reaction (-0.21 eV).

Fig. 4.13 shows the Gibbs energetics of step 2 in the x axis and the Gibbs energetics of step 1 as the y axis. To build the contour, the overpotential (Eq. 4.8) should be written solely as function of ΔG_1 and ΔG_2. This is show in Eq. 4.11:

$$\eta = \frac{\max(\Delta G_2, \Delta G_{rxn} - \Delta G_2 - \Delta G_1)}{e^-} - \Delta E^0 \quad (4.11)$$

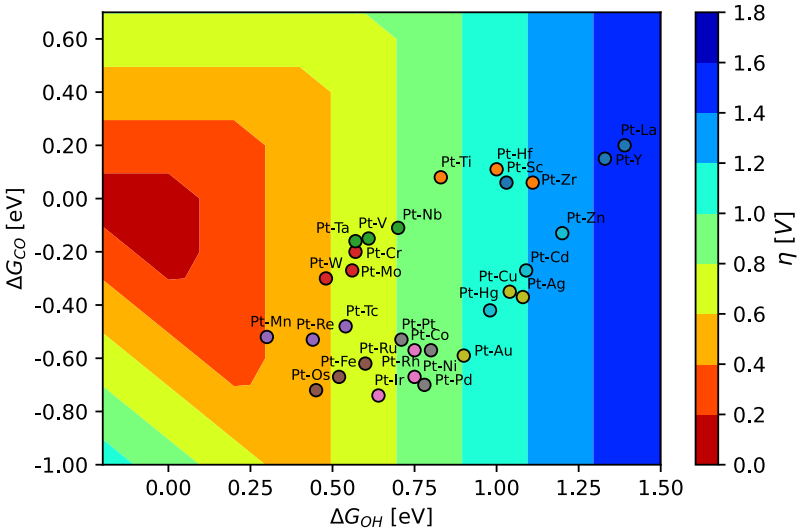

Figure 4.13. Volcano plot of the overpotential as a function of the *CO and *OH separate adsorption energies for a (111)-NSA. The optimal transition metal alloy is Pt-Mn. The colors used for the datapoints vary depending on the number of valence electrons of the guest atom.

Fig. 4.13 illustrates a series of ideas. First, it shows that Pt-Mn is probably the best transition metal for a (111) surface facet, while Pt-La and Pt-Y are the worst. In addition, the form of the contours is triangular, and all the points lie on the same side of the triangles. This provides valuable information about the reaction mechanism: if a data point is displaced vertically (that is, if *CO adsorption is modified) there would be no impact on the overpotential of the reaction. There would only be an impact if a point is moved horizontally (that is, if *OH adsorption is modified). This means that the reaction is controlled only by *OH adsorption. Note that this behavior was observed before in Fig. 4.4b.

Normally, for CO electro-oxidation, Pt-Ru bulk alloys are used to construct the electrodes [1], yet it is interesting to observe the catalytic improvement alloying provides with respect to pure Pt electrodes for the different alloys studied. From Fig. 4.11, it seems clear that there are several materials that may show a better catalytic activity. To quantify this, a normalized volcano plot with respect to Pt was constructed (Fig. 4.14). Instead of representing the overpotential, the

current with respect to that of Pt(111) is plotted. This quantity is linked to the overpotential as described in the theoretical background [11].

To construct such a volcano plot, a procedure similar to that of [16] is followed. The rate determining steps of the reaction must be identified, in this case steps 2 and steps 3. For both steps a Tafel Equation is written (Eq. 4.12-13) that relates the current to the overpotential.

$$j_L = j_0 \cdot \exp\left[\frac{-\beta \cdot \Delta G_3}{k_B \cdot T}\right] \quad (4.12)$$

$$j_R = j_0 \cdot \exp\left[\frac{-\beta \cdot \Delta G_2}{k_B \cdot T}\right] \quad (4.13)$$

An assumption this model makes is that the pre-factors of the right and left binding leg are the same. For this work, β is assumed to be 0.5, as customary for single electron transfers [11,22]. In these equations k_B corresponds to Boltzmann constant, while T refers to the absolute temperature, here in K.

To normalize the current with respect to Pt, the value of $\Delta G_{2\,Pt}$ is considered since Pt lies on the weak OH-binding leg. Eq. 4.13 can be rewritten as Eq. 4.14:

$$\frac{k_B \cdot T}{\beta} \cdot \ln \frac{j_R}{j_{Pt}} = \Delta G_{2\,Pt} - \Delta G_2 \quad (4.14)$$

For the strong OH-binding leg, a series of mathematical operations must be performed before a useful expression is obtained. They are shown through Eq. 4.15-17:

$$\frac{k_B \cdot T}{\beta} \cdot \ln \frac{j_L}{j_{Pt}} = \Delta G_{2\,Pt} - \Delta G_3 \quad (4.15)$$

$$\frac{k_B \cdot T}{\beta} \cdot \ln \frac{j_L}{j_{Pt}} = \Delta G_{2\,Pt} - \Delta G_{rx} + \Delta G_1 + \Delta G_2 \quad (4.16)$$

$$\frac{k_B \cdot T}{\beta} \cdot \ln \frac{j_L}{j_{Pt}} = -\Delta G_{rx} + 2 \cdot \Delta G_{2\,Pt} + \Delta G_{1\,Pt} + (\Delta G_1 - \Delta G_{1\,Pt}) + (\Delta G_2 - \Delta G_{2\,Pt}) \quad (4.17)$$

Eq. 4.16 and 4.17 are equivalent to each other, since the only mathematical operations performed are the addition and subtraction of $\Delta G_{1\,Pt}$ and $\Delta G_{2\,Pt}$, which does not alter the equation.

With Eq. 4.14 and 17, a 3d volcano plot that relates the normalized current as a function of $\Delta G_1 - \Delta G_{1\,Pt}$ and $\Delta G_2 - \Delta G_{2\,Pt}$ can be constructed. This volcano plot should exhibit the same

shape as that of Fig. 4.14. The reason is that the natural logarithm of the current relates linearly to the overpotential through the Tafel equation; however, the scale will not be the same.

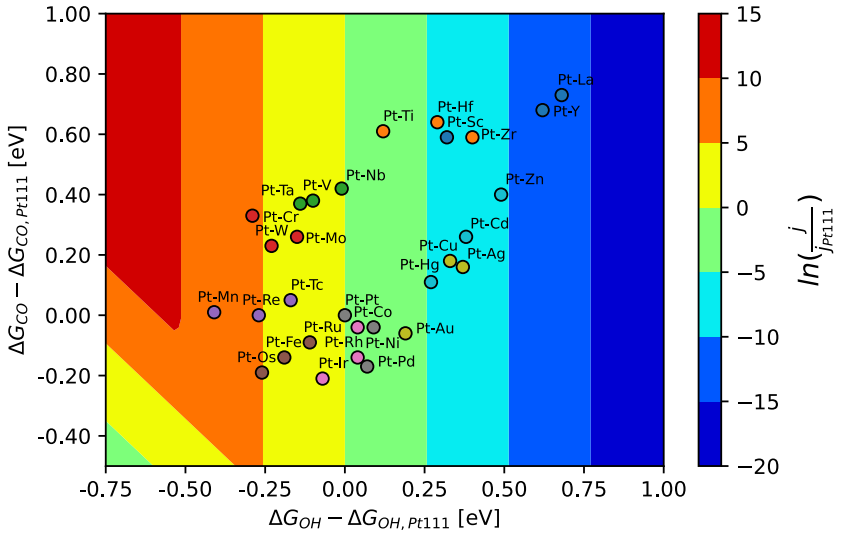

Figure 4.14. Volcano plot of the current density normalized with respect to that of Pt(111) as a function of *CO and *OH adsorption energies. The Pt-Mn (111)-NSA outperforms the Pt(111) by 3 orders of magnitude. The colors used for the datapoints vary depending on the number of valence electrons of the guest atom.

What has been previously said for Fig. 4.12 regarding the rate determining step also holds for this figure; however, this figure shows clearly how the catalysts perform with respect to pure Pt. Alloys to the left of pure Pt perform better, while those to the right perform worse. The (111) Pt-Mn NSA outperforms the pure Pt(111) electrode by 3 orders of magnitude. This shows that Pt-Mn (111) NSA is a promising material for CO electro-oxidation not only in terms of activity but also in terms of cost, since Mn is less expensive than Pt.

4.5. COVERAGE EFFECTS ON THE CATALYTIC ACTIVITIES

Up to this point, the catalyst has been modeled in a way such that the subsurface layer was completely covered by a guest transition metal. It is interesting to observe the effect of varying

the coverage of this metal for two reasons: firstly, altering the coverage could lower the overpotential for a given catalyst yielding better results, and secondly, building a catalyst with a complete monolayer is very difficult, since at least some of the guest atoms will probably diffuse through the surface layers into the bulk.

Evaluating the effect of the coverage for every surface studied would have required a massive amount of data to generate and analyze. For that reason, we only studied the case of Pt-Mn because it showed the best performance.

For this catalyst, the coverage can be varied from 0 (pure platinum) to 1 ML (Pt-Mn monolayer). For intermediate values (0.25, 0.5, 0.75 ML), all atop adsorption sites are not analogous, since they interact with a different number of Mn atoms. This is shown in Fig. 4.15:

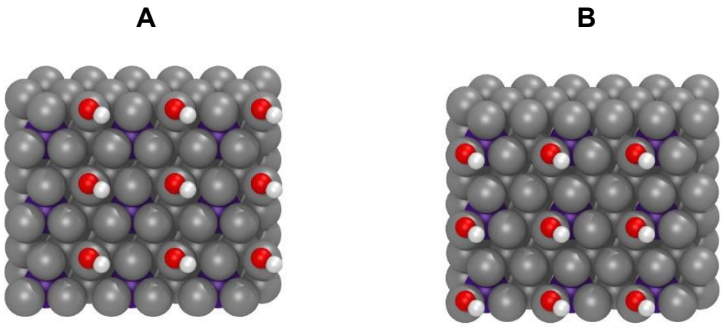

Figure 4.15. Geometric configuration of a (111) Pt-Mn NSA with a Mn coverage of 0.25 ML. The panels show the two possible configurations, where the Pt atom binding *OH has no Mn neighbors (A), while the other has one (B). The color code used is purple for Mn, silver for Pt, white for H, and red for O.

The reaction mechanism (Eq. 4.1-3) was simulated on these catalysts. From the results, the overpotential was calculated as done previously (Eq. 4.8). The overpotential was plotted as a function of the number of valence electrons in Fig. 4.16, and an inset was added to evince the effects of Mn coverage.

Fig. 4.16 shows a volcano plot for all the alloys analyzed. The inset shows a green point corresponding to a pure Pt alloy, while the blue one corresponds to a Pt-Mn alloy with 1 ML Mn

(both points are shown in the main panel). From the inset, two ideas can be extracted: first, the optimal coverage for Pt-Mn corresponds to a full monolayer. Second, the addition of Mn to Pt(111) is beneficial in terms of catalytic activity at any proportion. The increase in activity depends on the adsorption site and the coverage. It seems that as Mn becomes the predominant species in the second layer, the adsorption site with more Mn neighbors becomes more active; however, when Pt is the most predominant species then the most active sites are those with less Mn neighbors. The switch is found around 0.50-0.75 ML.

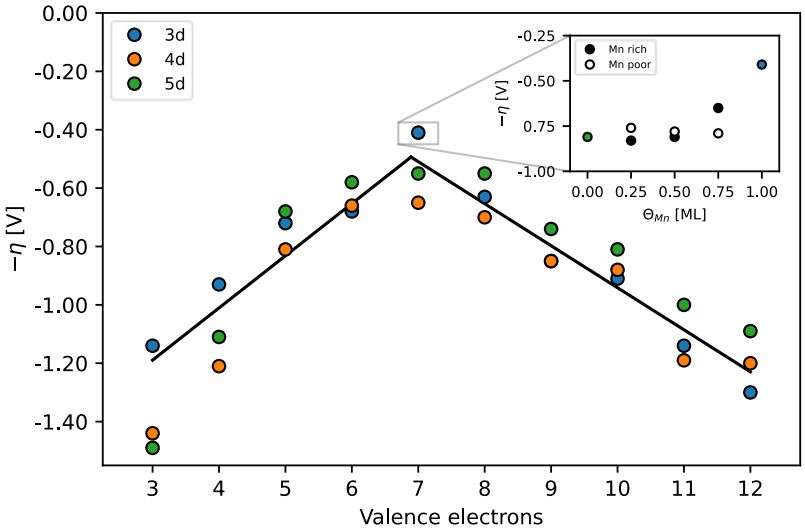

Figure 4.16. Activity-valence electron plot for all transition metals. Inset: Activity-Mn coverage plot. The optimal surface for a (111)-NSA is Pt-Mn with a Θ_{Mn} = 1 ML. The linear fits have a MAE of 0.09 eV and the lines have R values of at least 0.97.

5. CATALYTIC ACTIVITY OF NEAR-SURFACE ALLOYS OF PLATINUM (331) AND TRANSITION METALS

5.1. INTRODUCTION

When designing a catalyst there are several parameters one can tune. In the previous section, the catalytic activity was analyzed for a given surface (i.e. the (111) facet) and configuration (a NSA). In this section, the alloy configuration will remain the same, such that the guest atom will be put in the subsurface layer; however, the surface facet will be modified. The change from a (111) to a (331) surface implies a reduction of the coordination number of the active sites from 9 to 7, if step-edge atoms are studied on the latter. It is interesting to test what effect this coordination change implies, and whether the models utilized for the (111) surface still apply.

A Pt(331) NSA is a more complex surface model since it involves more atoms and the surface contains atoms of dissimilar coordination. When alloying with big atoms such as Sc, Ti, Y, Zr, La and Hf, convergence problems are encountered, and large surface reconstructions can be observed. For that reason, the analysis will only extend from 5 to 12 valence electrons. In Fig. 5.1, the structure of a (331) Pt-NSA is provided.

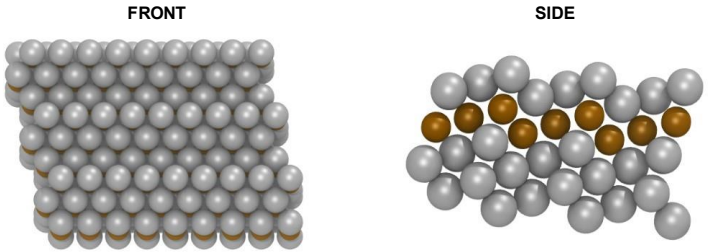

Figure 5.1. Geometric configuration of a (331) Pt-Cu NSA. Each subplot represents a different view of the same cell. The color code used is ochre for Cu, and silver for Pt.

The reaction mechanism remains the same (Eq. 4.1-3). For this surface, there is scientific evidence that the adsorbates bind at the step edges [9], in view of their lower surface coordination. With this information the adsorbates can be modeled, as shown in Fig. 5.2-3.

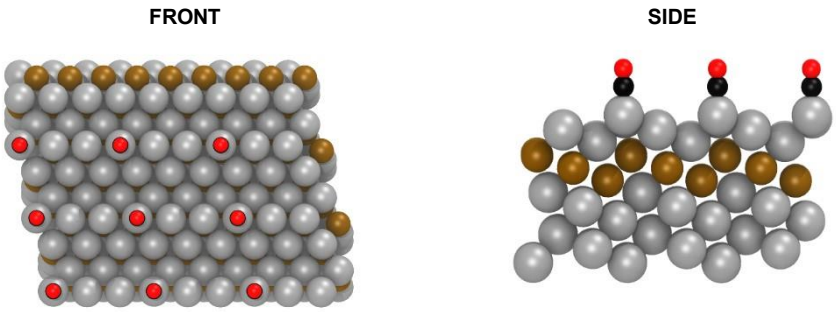

Figure 5.2. Structure of a (331) Pt-Cu NSA with *CO on the step edge. Each subplot represents a different view of the same cell. The color code used is ochre for Cu, silver for Pt, black for C and red for O.

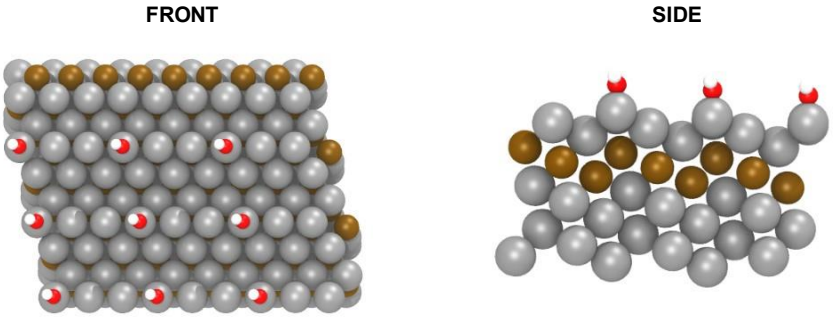

Figure 5.3. Structure of a (331) Pt-Cu NSA with *OH adsorbed on the step edge. Each subplot represents a different view of the same cell. The color code used is ochre for Cu, silver for Pt, white for H, and red for O.

5.2. ANALYSIS BASED ON THE NUMBER OF VALENCE ELECTRONS

The Gibbs free energies for each step and the overpotential are calculated as done for the (111) NSAs in the previous chapter. The energies are plotted as a function of the number of valence electrons (Fig. 5.4).

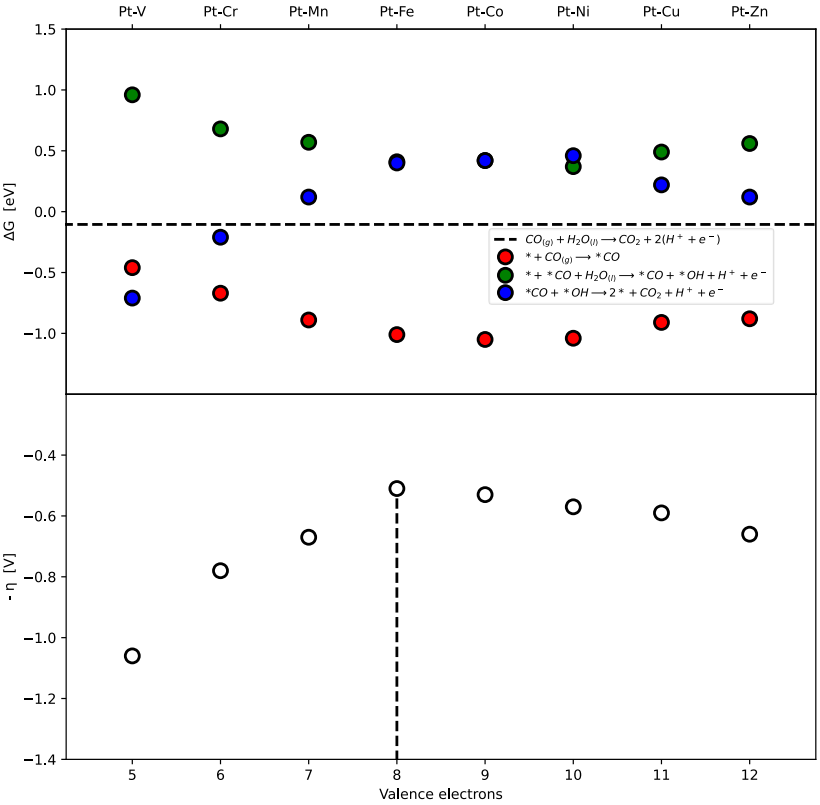

Figure 5.4. (a) Gibbs free energy for each step of the electro-oxidation of CO as a function of the valence number for (331)-NSAs of Pt and 3d metals. (b) Valence electron-activity plot for CO electro-oxidation. The optimal alloy has 8 valence electrons. The overpotential is calculated as $\eta = \frac{\max(\Delta G_2, \Delta G_3)}{e^-} - \Delta E^0$.

The results in Fig. 5.4 show differences with respect to those of on (111) surfaces. Everything discussed about Fig. 5.4 will also be true for 4d and 5d metals; see the figures in Appendix 2 (A.1, A.2). The reduction of the coordination number caused something that did not happen before, namely that for some alloys the reaction is hindered by *CO and *OH recombination (step 3).

The volcano plot from Fig. 5.4b shows that for the left side, the reaction is limited by weak *OH binding, while for the right side, the reaction is limited by strong *OH binding. The optimal catalyst according to the Sabatier principle is one that does not bind neither too strongly nor too weakly [7]. For the (331) surface facet, the optimal catalyst has 8 valence electrons (Fe), which corresponds to a shift of +1 electron with respect to (111) surfaces.

Furthermore, a close inspection of the energetics shows a different behavior with respect to (111) surfaces. Previously, there was a steep decrease in both *OH and *CO adsorption until approximately 6 valence electrons. However, once the minima were achieved (7 e^- for *OH and 8 e^- for CO), the alloys experienced an increase in adsorption energies. The energetic behavior for low values of valence electrons seems to be identical to that of (111) surfaces; nonetheless, for high values the energetic increase is more subtle.

For (331) NSAs, the use of the 8 and 18 electron rules do not seem to apply in a straightforward manner. Since the reaction has not changed, the minima for both *CO and *OH adsorption should remain the same (7 e^- for *OH, 8 e^- for *CO). However, when these energies are plotted as function of the number of valence electrons (Fig. 5.5-6), for all transition metal series, and regardless of the adsorbate chosen, the minima correspond to 10 valence electrons. This could imply that the interactions between Pt and the guests are not as strong as for a (111) surface. In this case, the fact that the minima lie at 10 valence electrons could be due to coordination effects masking ligand effects.

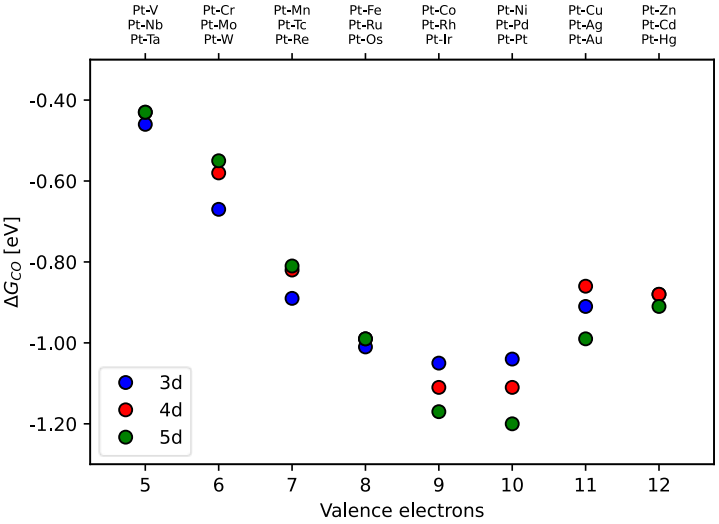

Figure 5.5. Adsorption energy of *CO for alloys of different d series. The minimal CO adsorption energy corresponds to 10 valence electrons for 3d,4d and 5d transition metals.

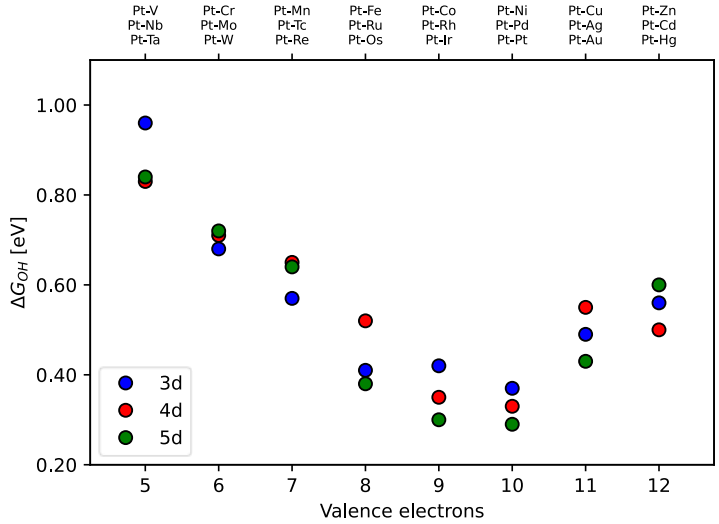

Figure 5.6. Adsorption energy of *OH for alloys of different d series. The minimal *OH adsorption energy corresponds to 10 valence electrons for 3d, 4d, 5d transition metals.

5.3. ANALYSIS BASED ON SCALING RELATIONS

Since the energetic curves share the same extrema (in this case, the same minima), it is expected to observe a linear scaling between adsorbates [14]. This would have significant advantages for the elaboration of activity plots, since the overpotential can be drawn as a function of only one adsorption energy. However, it also imposes a maximum theoretical efficiency since the energetics must lie somewhere along the scaling line. Following the procedure for the (111) surfaces, the Gibbs energy of *OH adsorption is plotted as a function of that of *CO adsorption.

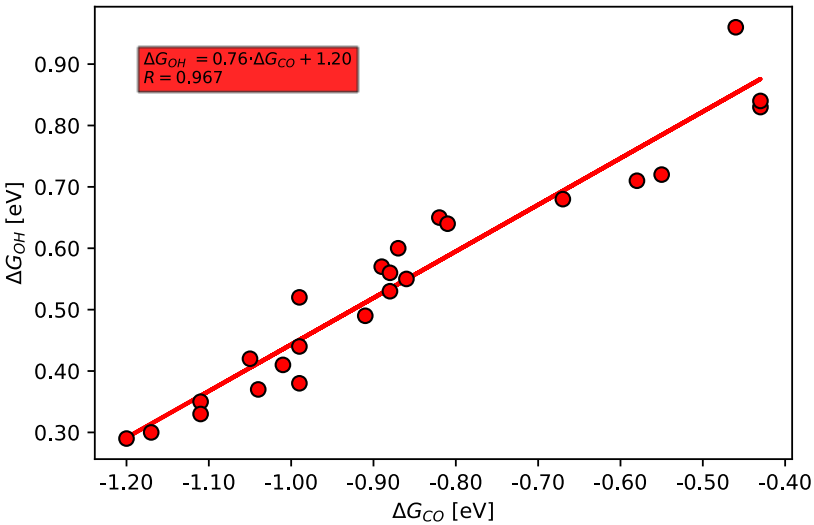

Figure 5.7. Scaling relation for the adsorption energies of *CO and *OH on NSAs of Pt(331). The linear scaling model shows a R value of 0.967.

Since correlation in Fig. 5.7 is approximately a straight line, *CO and *OH are linearly dependent on this facet. Scaling relations have been studied in detail [21,23,24], and it is known that the slope of the lines is the quotient between the number of bonds each adsorbate is lacking to reach the octet [7,14]. For this surface, the slope should be around ½, but it is instead 0.76. One idea that comes to mind that could explain this is that CO binds differently to the surface. CO can bind through a single or double bond, which would yield different slopes (1 and

½, respectively). The value observed is 0.76, which is very similar to the mean between 1 and 1/2 (0.75).

The activity of this surface can be studied more easily now since it is no longer necessary to make a 3D volcano plot. Now the overpotential can be exclusively linked to the Gibbs free energy of *OH adsorption. To do so, Eq. 4.8 and the linear fit from Fig. 5.7 are combined (Eq. 5.1).

$$\eta=\max(1.22\ \Delta G_{OH}-1.53,\Delta G_{OH},\Delta G_{rxn}-2.22\ \Delta G_{OH}+1.53) \quad (5.1)$$

This shows the power of scaling relations, since now it is only necessary to do one calculation (i.e. *OH adsorption) to swiftly predict how good a catalyst is. The result of plotting the overpotential as a function of the Gibbs free energy of *OH adsorption is shown in Fig. 5.8.

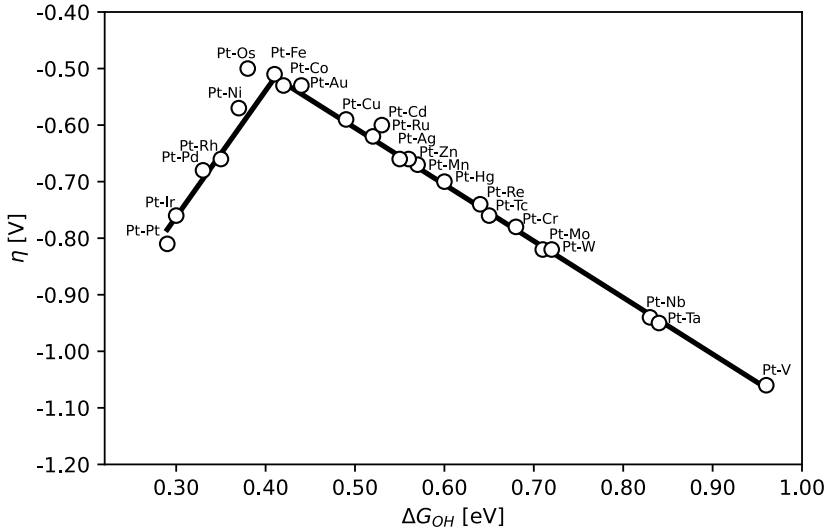

Figure 5.8. Overpotential for CO oxidation as a function of the Gibbs free energy of *OH. The optimal catalyst for a (331)-NSA is made of platinum and osmium. CO electro-oxidation is predicted to experience low overpotentials for catalysts with ΔG_{OH} around 0.4 eV.

From Figure 5.8, it seems clear that the optimal catalyst for this surface is the (331) Pt-Os NSA, but there are several candidates with similar activities. The selection of one of these catalysts over the other will probably depend on the overall production costs. In addition, Pt-Au

is a catalyst with excellent predicted activity, which has a significantly higher number of valence electrons than others close to the top of the volcano.

Lastly, the activity of this surface was quantified with respect to pure platinum, just as it was done for the (111) surfaces. The procedure is analogous to the one in chapter 4 but now scaling relations can be used, so that a 2D volcano can be made. In this case, we normalized with respect to Pt(331). The rate determining steps remain the same as for (111) surfaces; therefore, Eq. 4.12-13 still apply. The difference is that now Pt is on the strong *OH binding side, thus the equation for the left-hand side of the volcano after a series of mathematical operations is Eq. 5.5:

$$\frac{k_B \cdot T}{\beta} \ln \frac{j_L}{j_{Pt}} = \Delta G_{3\,Pt} - \Delta G_3 \tag{5.2}$$

$$\frac{k_B \cdot T}{\beta} \cdot \ln \frac{j_L}{j_{Pt}} = \Delta G_{3\,Pt} - \Delta G_{rx} + \Delta G_1 + \Delta G_2 \tag{5.3}$$

$$\frac{k_B \cdot T}{\beta} \cdot \ln \frac{j_L}{j_{Pt}} = \Delta G_{3\,Pt} - \Delta G_{rx} + \gamma \cdot \Delta G_2 + \varepsilon + \Delta G_2 \tag{5.4}$$

$$\frac{k_B \cdot T}{\beta} \cdot \ln \frac{j_L}{j_{Pt}} = \Delta G_{3\,Pt} - \Delta G_{rx} + \Delta G_{2\,Pt} + \varepsilon + (\gamma+1) \cdot \Delta G_2 - \Delta G_{2\,Pt} \tag{5.5}$$

For the right side of the volcano, the derivation of the equation is similar, except that on this side of the volcano the reaction is hindered by *OH adsorption:

$$\frac{k_B \cdot T}{\beta} \cdot \ln \frac{j_L}{j_{Pt}} = \Delta G_{3\,Pt} - \Delta G_2 \tag{5.6}$$

$$\frac{k_B \cdot T}{\beta} \cdot \ln \frac{j_L}{j_{Pt}} = \Delta G_{3\,Pt} - \Delta G_{2\,Pt} - \Delta G_2 + \Delta G_{2\,Pt} \tag{5.7}$$

With Eq. 5.5 and 5.7, a normalized volcano plot can be made that quantifies the increase and decrease of activity with respect to a pure Pt(331) electrode. The results in Fig. 5.9 indicate that a (331) Pt-Fe NSA has the greatest catalytic power among all the alloys simulated, and Pt-Au or Pt-Co NSAs are also fairly active. This happens because Pt-Os does not fit well the correlation, if it did, it would be at the top of the volcano. Through these equations (Eq. 5.5 and 5.7), it can be quantified that the current density of a (331) Pt-Fe NSA is larger than those of

Pt(331) by 2 orders of magnitude. The improvement is significant but not as much as for the (111) Pt-Mn NSA reported in chapter 4.

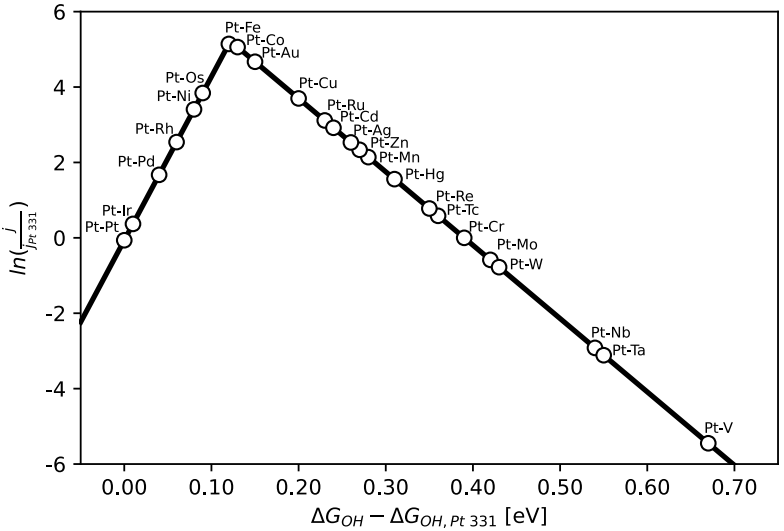

Figure 5.9. Volcano plot of the current density normalized with respect to that of Pt(331) as a function of *OH adsorption energies. The Pt-Fe (331)-NSA outperforms the Pt(331)-NSA by 2 orders of magnitude.

6. CONCLUSIONS AND OUTLOOK

This research project aimed to determine promising materials for CO electro-oxidation, as well as to observe the effect of lowering the coordination number of the active sites. From the results presented in chapters 4 and 5 the following can be concluded:

- The best catalyst among all the alloys studied is the (111) Pt-Mn NSA with an overpotential of 0.41 V.
- For the (331) surfaces, the best alloy is the (331) Pt-Os NSA with an overpotential is 0.50 V. Nonetheless, it is not as active as the (111) Pt-Mn NSA.
- For the (111) NSAs, coadsorption calculations shift the energies by approximately 0.1 eV.
- The (111)-NSAs do not exhibit linear scalability between *CO and *OH. In view of that, 3D volcano plots were constructed. The plots show that *OH adsorption hinders the reaction, and future research could be focused on finding surfaces with more favorable binding energies.
- The (331)-NSAs display linear scalability between *OH and *CO. This feature was seized for a facile search of optimal materials, via simplified microkinetic models and volcano plots. The plots show that the mechanism is controlled by either *OH adsorption or CO_2 production, depending on the catalyst.

This thermodynamic analysis of catalysts has been shown to be very useful at predicting catalytic activities [7]. However, the actual pathway a reaction mechanism follows does not only depend on the thermodynamics, but on kinetics as well. For that reason, future efforts should be dedicated toward solving an advanced microkinetic model for the mechanism proposed (Eq. 4.1-3).

REFERENCES AND NOTES

[1] P. Breeze, “Direct Methanol Fuel Cell,” in Fuel Cells, Elsevier, 2017. doi: 10.1016/B978-0-08-101039-6.00008-X.

[2] Y. N. Sudhakar, M. Selvakumar, and D. K. Bhat, “Biopolymer Electrolytes for Fuel Cell Applications,” in Biopolymer Electrolytes, Elsevier, 2018. doi: 10.1016/B978-0-12-813447-4.00005-4.

[3] Sholl. David and J. Steckel, “DENSITY FUNCTIONAL THEORY: A Practical Introduction,” New Jersey: John Wiley & Sons, 2009, pp. 1–30.

[4] Georg Kresse, Martijn Marsman, and Jürgen Furthmüller, VASP the GUIDE. Vienna, 2018. Accessed: May 12, 2021. [Online]. Available: http://cms.mpi.univie.ac.at/vasp/vasp.pdf

[5] P. Atkins and J. de Paula, “Elements of Physical Chemistry,” 7th ed., Oxford University Press, 2017, pp. 177–184.

[6] P. Atkins and J. de Paula, “Elements of Phyiscal Chemistry,” 7th ed., Oxford: Oxford University Press, 2017, pp. 230–232.

[7] F. Calle-Vallejo and M. T. M. Koper, “First-principles computational electrochemistry: Achievements and challenges,” Electrochimica Acta, vol. 84, Dec. 2012, doi: 10.1016/j.electacta.2012.04.062.

[8] D. Lide, “CRC Handbook of Chemistry and Physics,” 84th ed., CRC Press, 2003.

[9] F. Calle-Vallejo, M. D. Pohl, and A. S. Bandarenka, “Quantitative Coordination–Activity Relations for the Design of Enhanced Pt Catalysts for CO Electro-oxidation,” ACS Catalysis, vol. 7, no. 7, Jul. 2017, doi: 10.1021/acscatal.7b01105.

[10] F. Calle-Vallejo and M. T. M. Koper, “Theoretical Considerations on the Electroreduction of CO to C 2 Species on Cu(100) Electrodes,” Angewandte Chemie International Edition, vol. 52, no. 28, Jul. 2013, doi: 10.1002/anie.201301470.

[11] Y.-H. Fang and Z.-P. Liu, “Tafel Kinetics of Electrocatalytic Reactions: From Experiment to First-Principles,” ACS Catalysis, vol. 4, no. 12, Dec. 2014, doi: 10.1021/cs501312v.

[12] K. Scott and L. Xing, “Direct Methanol Fuel Cells,” 2012. doi: 10.1016/B978-0-12-386874-9.00005-1.

[13] G. Rayner-Canham and T. Overton, “Descriptive Inorganic Chemistry,” 5th ed., New York: Freeman and Company, 2010, pp. 24–27.

[14] F. Calle-Vallejo, J. I. Martínez, J. M. García-Lastra, J. Rossmeisl, and M. T. M. Koper, “Physical and Chemical Nature of the Scaling Relations between Adsorption Energies of Atoms on Metal Surfaces,” Physical Review Letters, vol. 108, no. 11, Mar. 2012, doi: 10.1103/PhysRevLett.108.116103.

[15] A. S. Bandarenka et al., “Design of an Active Site towards Optimal Electrocatalysis: Overlayers, Surface Alloys and Near-Surface Alloys of Cu/Pt((111)),” Angewandte Chemie International Edition, vol. 51, no. 47, Nov. 2012, doi: 10.1002/anie.201205314.

[16] V. Viswanathan, H. A. Hansen, J. Rossmeisl, and J. K. Nørskov, “Universality in Oxygen Reduction Electrocatalysis on Metal Surfaces,” ACS Catalysis, vol. 2, no. 8, Aug. 2012, doi: 10.1021/cs300227s.

[17] G. Kresse and D. Joubert, “From ultrasoft pseudopotentials to the projector augmented-wave method,” Physical Review B, vol. 59, no. 3, Jan. 1999, doi: 10.1103/PhysRevB.59.1758.

[18] G. Kresse and J. Furthmüller, “Efficient iterative schemes for ab initio total-energy calculations using a plane-wave basis set,” Physical Review B, vol. 54, no. 16, Oct. 1996, doi: 10.1103/PhysRevB.54.11169.

[19] J. P. Perdew, K. Burke, and M. Ernzerhof, “Generalized Gradient Approximation Made Simple,” *Physical Review Letters*, vol. 77, no. 18, Oct. 1996, doi: 10.1103/PhysRevLett.77.3865.

[20] H. J. Monkhorst and J. D. Pack, “Special points for Brillouin-zone integrations,” Physical Review B, vol. 13, no. 12, Jun. 1976, doi: 10.1103/PhysRevB.13.5188.

[21] F. Abild-Pedersen *et al.*, “Scaling Properties of Adsorption Energies for Hydrogen-Containing Molecules on Transition-Metal Surfaces,” *Physical Review Letters*, vol. 99, no. 1, Jul. 2007, doi: 10.1103/PhysRevLett.99.016105.

[22] R. Guidelli et al., “Defining the transfer coefficient in electrochemistry: An assessment (IUPAC Technical Report),” Pure and Applied Chemistry, vol. 86, no. 2, Feb. 2014, doi: 10.1515/pac-2014-5026.

[23] F. Calle-Vallejo, D. Loffreda, M. T. M. Koper, and P. Sautet, “Introducing structural sensitivity into adsorption–energy scaling relations by means of coordination numbers,” Nature Chemistry, vol. 7, no. 5, May 2015, doi: 10.1038/nchem.2226.

[24] H.-Y. Su, K. Sun, W.-Q. Wang, Z. Zeng, F. Calle-Vallejo, and W.-X. Li, “Establishing and Understanding Adsorption–Energy Scaling Relations with Negative Slopes,” The Journal of Physical Chemistry Letters, vol. 7, no. 24, Dec. 2016, doi: 10.1021/acs.jpclett.6b0243

[25] P. Atkins and J. de Paula, “Elements of Phyiscal Chemistry,” 7th ed., Oxford: Oxford University Press, 2017, pp. 230–232.

[26] W. Wang, X. Wei, D. Choi, X. Lu, G. Yang, and C. Sun, “Electrochemical cells for medium- and large-scale energy storage,” in Advances in Batteries for Medium and Large-Scale Energy Storage, Elsevier, 2015. doi: 10.1016/B978-1-78242-013-2.00001-7.

[27] P. Strasser et al., “Lattice-strain control of the activity in dealloyed core–shell fuel cell catalysts,” Nature Chemistry, vol. 2, no. 6, Jun. 2010, doi: 10.1038/nchem.623.

APPENDICES

APPENDIX 1: DATA FOR FIGURES IN CHAPTER 4

To make the figures in Chapter 4, it is required to know the energetics of the molecules, the adsorbates, the zero-point energy corrections (ZPE), and the solvation energy [9,10]. For the molecules, the energies of formation, the ZPE and the solvation energy are available in Table1. For the adsorption of *CO and *OH the values are in Table 2. For the coadsorption model, the energies are available in Table 3. Lastly, in Table 4, we provide the ZPE corrections for every alloy for the adsorption and co-adsorption model.

Table 1. Molecule energetics, as well as adsorbate corrections.

Species	ZPE [eV]	TS [eV]	Esolv [eV]
CO (g)	0.13	0.61	0.00
CO_2 (g)	0.31	0.66	0.00
H_2 (g)	0.28	0.40	0.00
H_2O (l)	0.58	0.67	0.00
*OH	0.33	0.00	-0.58
*CO	0.21	0.00	-0.10

Table 2. Adsorption Energies for the (111) NSAs.

Alloys	ΔE_{CO} [eV]	ΔE_{OH} [eV]
Pt-Sc	-0.75	1.25
Pt-Ti	-0.73	1.05
Pt-V	-0.96	0.83
Pt-Cr	-1.02	0.64
Pt-Mn	-1.34	0.52
Pt-Fe	-1.49	0.74
Pt-Co	-1.39	0.98
Pt-Ni	-1.40	1.03

Pt-Cu	-1.17	1.26
Pt-Zn	-0.94	1.43
Pt-Y	-0.66	1.56
Pt-Zr	-0.76	1.34
Pt-Nb	-0.93	0.93
Pt-Mo	-1.09	0.78
Pt-Tc	-1.30	0.76
Pt-Ru	-1.44	0.81
Pt-Rh	-1.50	0.96
Pt-Pd	-1.53	0.99
Pt-Ag	-1.19	1.31
Pt-Cd	-1.09	1.32
Pt-La	-0.60	1.61
Pt-Hf	-0.70	1.23
Pt-Ta	-0.98	0.80
Pt-W	-1.12	0.70
Pt-Re	-1.36	0.65
Pt-Os	-1.54	0.66
Pt-Ir	-1.57	0.85
Pt-Pt	-1.36	0.92
Pt-Au	-1.41	1.12
Pt-Hg	-1.24	1.20

Table 3. Coadsorption energies for (111) NSAs.

Alloys	ΔE_{CO} [eV]	ΔE_{OH} [eV]
Pt-Sc	-0.75	1.23
Pt-Ti	-0.73	1.02
Pt-V	-0.96	0.93
Pt-Cr	-1.02	0.74
Pt-Mn	-1.34	0.81
Pt-Fe	-1.49	0.89
Pt-Co	-1.39	1.07

Pt-Ni	-1.40	1.15
Pt-Cu	-1.17	1.37
Pt-Zn	-0.94	1.49
Pt-Y	-0.66	1.59
Pt-Zr	-0.76	1.35
Pt-Nb	-0.93	0.96
Pt-Mo	-1.09	0.87
Pt-Tc	-1.30	0.85
Pt-Ru	-1.44	0.95
Pt-Rh	-1.50	1.06
Pt-Pd	-1.53	1.07
Pt-Ag	-1.19	1.42
Pt-Cd	-1.09	1.37
Pt-Hf	-0.70	1.20
Pt-Ta	-0.98	0.86
Pt-W	-1.12	0.78
Pt-Re	-1.36	0.79
Pt-Os	-1.54	0.83
Pt-Ir	-1.57	0.97
Pt-Pt	-1.36	1.04
Pt-Au	-1.41	1.23
Pt-Hg	-1.24	1.21

Table 4. Zero-point energy corrections for adsorption and coadsorption.

Alloys	ZPE_{CO} [eV]	ZPE_{OH} [eV]	$ZPE_{CO\&OH}$ [eV]
Pt-Sc	0.20	0.32	0.53
Pt-Ti	0.20	0.32	0.53
Pt-V	0.20	0.33	0.54
Pt-Cr	0.21	0.33	0.55
Pt-Mn	0.21	0.33	0.55
Pt-Fe	0.21	0.33	0.56
Pt-Co	0.21	0.33	0.56
Pt-Ni	0.21	0.33	0.56

Pt-Cu	0.21	0.33	0.55
Pt-Zn	0.20	0.32	0.54
Pt-Y	0.19	0.32	0.52
Pt-Zr	0.20	0.32	0.53
Pt-Nb	0.20	0.32	0.54
Pt-Mo	0.20	0.33	0.54
Pt-Tc	0.21	0.33	0.55
Pt-Ru	0.21	0.34	0.55
Pt-Rh	0.21	0.34	0.56
Pt-Pd	0.21	0.34	0.56
Pt-Ag	0.20	0.33	0.55
Pt-Cd	0.20	0.32	0.54
Pt-La	0.19	0.32	0.00
Pt-Hf	0.20	0.32	0.53
Pt-Ta	0.20	0.32	0.54
Pt-W	0.20	0.33	0.54
Pt-Re	0.21	0.34	0.56
Pt-Os	0.21	0.34	0.56
Pt-Ir	0.21	0.34	0.56
Pt-Pt	0.21	0.34	0.57
Pt-Au	0.21	0.34	0.56
Pt-Hg	0.21	0.33	0.55

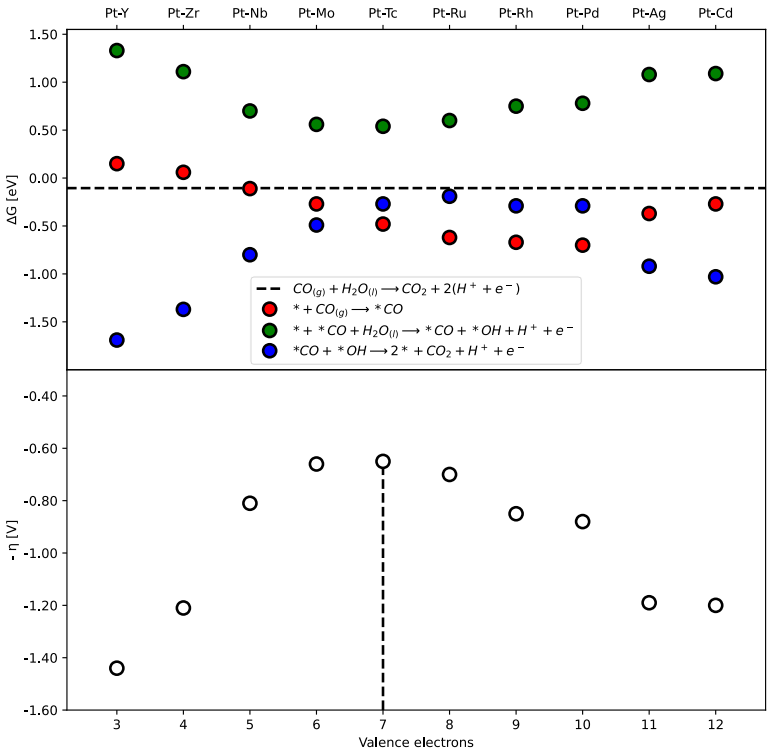

Figure A.1. (a) Gibbs free energy for each step of the electro-oxidation of CO as a function of the number of valence electrons for (111)-NSAs of Pt and 4d metals. (b) Valence electron-activity plot for CO electro-oxidation. The optimal alloy has 7 valence electrons. The overpotential is calculated as $\eta = \frac{\max(\Delta G_2, \Delta G_3)}{e^-} - \Delta E^0$.

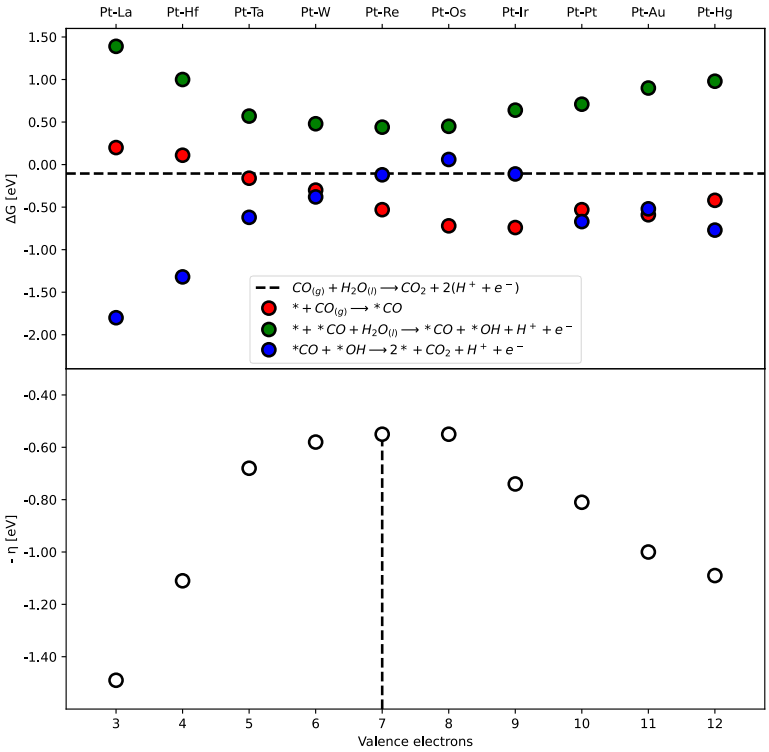

Figure A.2. (a) Gibbs free energy for each step of the electro-oxidation of CO as a function of the number of valence electrons for (111)-NSAs of Pt and 5d metals. (b) Valence electron-activity plot for CO electro-oxidation. The optimal alloy has 7 valence electrons. The overpotential is calculated as shown: $\eta = \frac{\max(\Delta G_2, \Delta G_3)}{e^-} - \Delta E^0$.

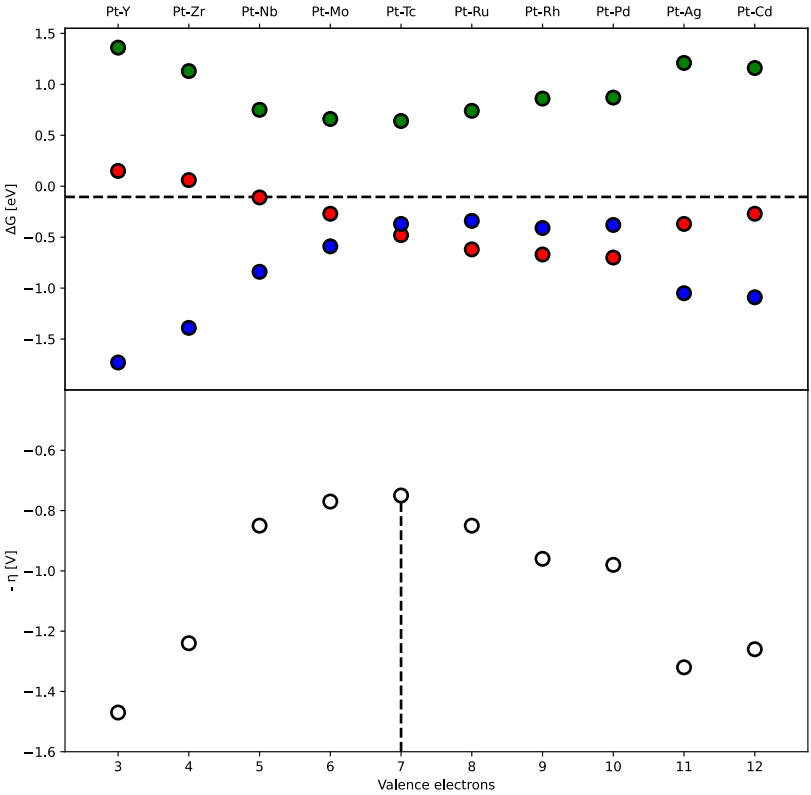

Figure A.3. (a) Gibbs free energy for each step of the electro-oxidation of CO as a function of the number of valence electrons for (111)-NSAs of Pt and 4d metals considering adsorbate interactions. (b) Valence electron-activity plot for CO electro-oxidation considering adsorbate interactions. The optimal alloy has 7 valence electrons. The overpotential is calculated as shown $\eta = \frac{\max(\Delta G_2, \Delta G_3)}{e^-} - \Delta E^0$.

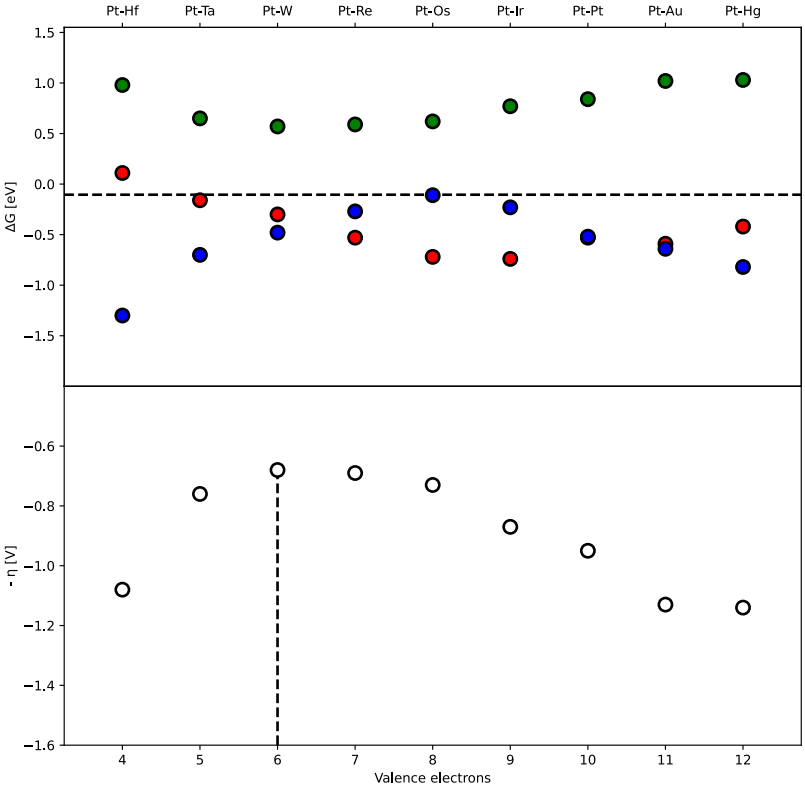

Figure A.4. (a) Gibbs free energy for each step of the electro-oxidation of CO as a function of the number of valence electrons for (111)-NSAs of Pt and 5d metals considering adsorbate interactions. (b) Valence electron-activity plot for CO electro-oxidation considering adsorbate interactions. The optimal alloy has 6 valence electrons. The overpotential is calculated as shown: $\eta = \frac{\max(\Delta G_2, \Delta G_3)}{e^-} - \Delta E^0$.

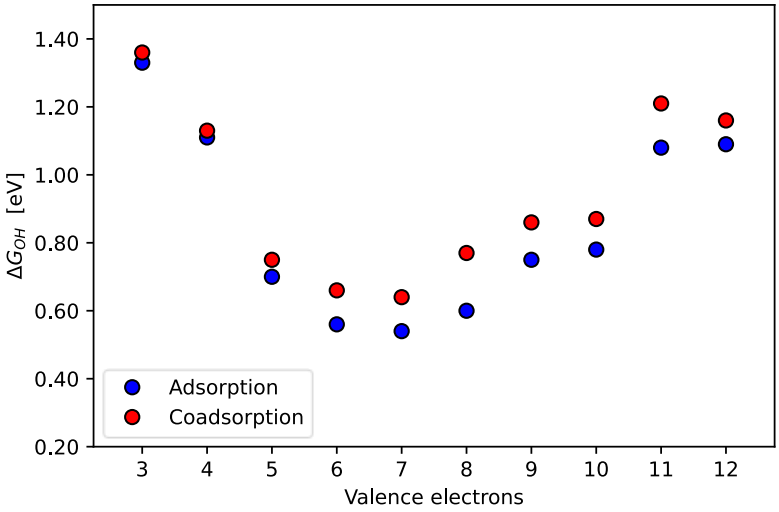

Figure A.5. Comparison between OH adsorption and OH coadsorption energy for NSAs of Pt and 4d transition metals. There is on average a constant energetic shift of 0.09 eV.

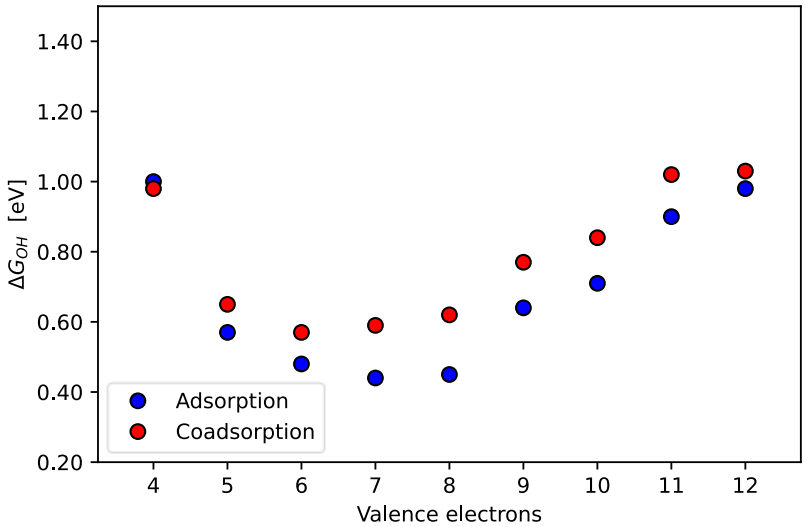

Figure A.6. Comparison between OH adsorption and *OH coadsorption with *CO for NSAs of Pt and 4d transition metals. There is on average a constant energetic shift of 0.09 eV.

APPENDIX 2: DATA FOR FIGURES IN CHAPTER 5

To construct the figures in Chapter 5, it is required to know the energetics of the adsorbates at a (331) NSA. The data for the molecules (Table 1) is the same as in the Appendix 1. The information regarding the adsorption energies is tabulated in Table 5, while the zero-point energy corrections (ZPE) are available in Table 6.

Table 5. Adsorption Energies for (331) NSAs.

Alloys	ΔE_{CO} [eV]	ΔE_{OH} [eV]
Pt-V	-1.27	0.96
Pt-Cr	-1.49	0.68
Pt-Mn	-1.71	0.57
Pt-Fe	-1.84	0.41
Pt-Co	-1.87	0.42
Pt-Ni	-1.87	0.37
Pt-Cu	-1.74	0.49
Pt-Zn	-1.70	0.56
Pt-Nb	-1.25	1.07
Pt-Mo	-1.40	0.93
Pt-Tc	-1.64	0.89
Pt-Ru	-1.81	0.75
Pt-Rh	-1.93	0.56
Pt-Pd	-1.94	0.54
Pt-Ag	-1.68	0.76
Pt-Cd	-1.70	0.76
Pt-Ta	-1.24	1.07
Pt-W	-1.37	0.93
Pt-Re	-1.64	0.88
Pt-Os	-1.81	0.59
Pt-Ir	-2.00	0.52
Pt-Pt	-2.03	0.50

Pt-Au	-1.81	0.65
Pt-Hg	-1.69	0.81

Table 6. Zero-point energy corrections for (331) NSAs.

Alloys	ZPE_{CO} [eV]	ZPE_{OH} [eV]
Pt-V	0.20	0.35
Pt-Cr	0.20	0.32
Pt-Mn	0.21	0.31
Pt-Fe	0.21	0.34
Pt-Co	0.21	0.33
Pt-Ni	0.21	0.33
Pt-Cu	0.21	0.33
Pt-Zn	0.20	0.33
Pt-Nb	0.20	0.32
Pt-Mo	0.20	0.34
Pt-Tc	0.21	0.31
Pt-Ru	0.21	0.32
Pt-Rh	0.21	0.34
Pt-Pd	0.21	0.34
Pt-Ag	0.21	0.34
Pt-Cd	0.21	0.33
Pt-Ta	0.20	0.32
Pt-W	0.20	0.34
Pt-Re	0.21	0.31
Pt-Os	0.21	0.34
Pt-Ir	0.21	0.33
Pt-Pt	0.21	0.34
Pt-Au	0.21	0.34
Pt-Hg	0.21	0.34

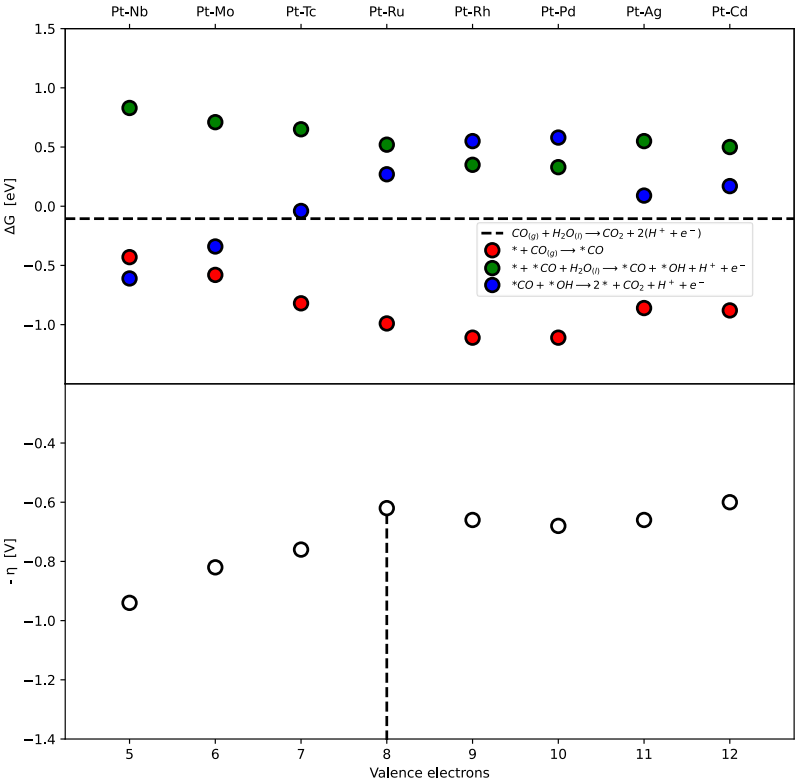

Figure A.1. (a) Gibbs free energy for each step of the electro-oxidation of CO as a function of the number of valence electrons for (111)-NSAs composed of Pt and 4d metals. (b) Valence electron-activity plot for CO electro-oxidation. The optimal alloy has 8 valence electrons. The overpotential is calculated as $\eta = \frac{\max(\Delta G_2, \Delta G_3)}{e^-} - \Delta E^0$.

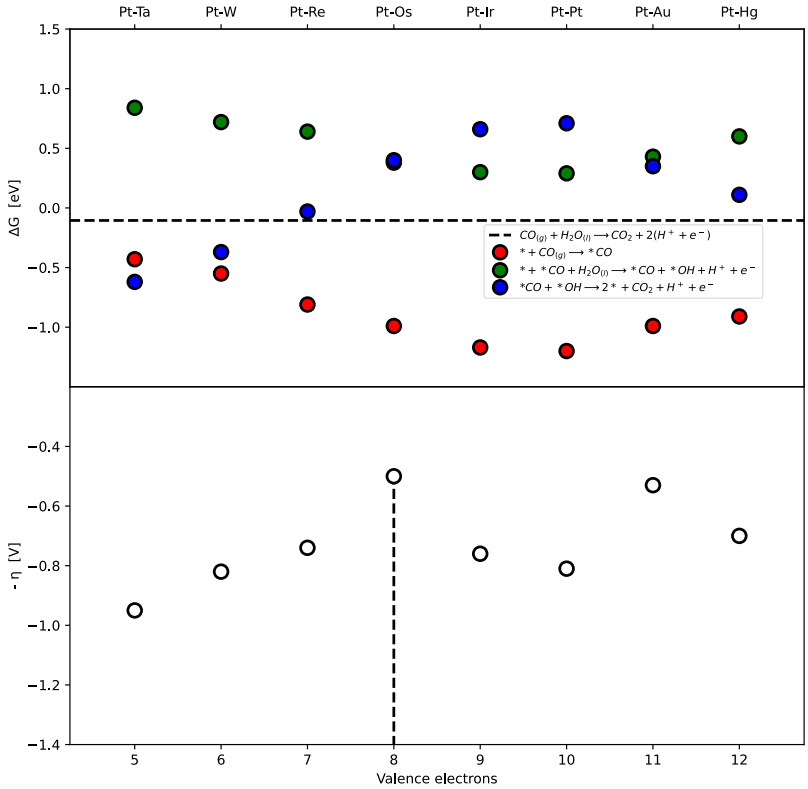

Figure A2.2. (a) Gibbs free energy for each step of the electro-oxidation of CO as a function of the number of valence electrons for (111)-NSAs of Pt and 5d metals. (b) Valence electron-activity plot for CO electro-oxidation. The optimal alloy has 8 valence electrons. The overpotential is calculated as $\eta = \frac{\max(\Delta G_2, \Delta G_3)}{e^-} - \Delta E^0$.